Pergamon

Geochimica et Cosmochimica Acta, Vol. 67, No. 9, pp. 1635–1658, 2003

0016-7037/03 $30.00 + .00

doi:10.1016/S0016-7037(00)00059-0

Mass-independent isotope effects in Archean (2.5 to 3.8 Ga) sedimentary sulfides determined by ion microprobe analysis

S. J. Mojzsis,[1,2,*] C. D. Coath,[1] J. P. Greenwood,[2] K. D. McKeegan,[1] and T. M. Harrison[1,2]
[1]Department of Earth and Space Sciences, University of California, Los Angeles, CA 90095-1567, USA
[2]Institute for Geophysics and Planetary Physics, University of California, Los Angeles, CA 90095-1567, USA

(*Received July* 1, 2002; *accepted in revised form December* 5, 2002)

Abstract—We report sulfur isotope anomalies with $\Delta^{33}S$, the deviation from a mass-dependent fractionation line for the three-isotope system ($^{34}S/^{32}S$ vs. $^{33}S/^{32}S$), ranging up to ±2‰ within individual Archean sedimentary sulfides from a variety of localities. Our measurements, which are made in situ by multicollector secondary ion mass spectrometry, unequivocally corroborate prior bulk measurements of mass-independent fractionations (MIF) in sulfur and provide additional evidence for an anoxic atmosphere on the Earth before ~2 Ga. This technique also offers new opportunities for exploring ancient sulfur metabolisms preserved in the rock record. The presence of MIF sulfur in sulfides from a >3.8-Ga Fe-rich quartzite from Akilia (island), West Greenland, is consistent with a marine sedimentary origin for this rock. *Copyright © 2003 Elsevier Science Ltd*

1. INTRODUCTION

The record of sulfur isotopic variability has long been recognized as a powerful tracer for investigating igneous, metamorphic, sedimentary, hydrothermal, and biologic processes on Earth (Thode et al., 1949). Sulfur is an abundant element in marine systems (standard seawater $[SO_4^{-}]_{aq} = 29$ mM; Millero and Sohn, 1992), and it has been utilized extensively as evidence for biogenicity in sediments spanning the geologic record (Goodwin et al., 1976; Monster et al., 1979; Schidlowski et al., 1983; Schidlowski, 1989). The sulfur isotope geochemistry of ancient sediments is used to explore fundamental questions related to the early Earth, such as tracing the evolution of sulfur metabolism and the appearance of sulfate-reducing bacteria (Monster et al., 1979; Schidlowski et al., 1983; Canfield and Raiswell, 1999; Shen et al., 2001). More recently, it has been argued that the sulfur isotope record has direct implications for tracing the rise of free oxygen in the atmosphere (Berner and Petsch, 1998; Farquhar et al., 2000, 2001a; Thiemens et al., 2001; Pavlov and Kasting, 2002).

Sulfur isotope compositions are expressed in the conventional δ notation as

$$\delta^{34}S_{CDT}\ (‰) = (R^{34}{}_{sample}/R^{34}{}_{CDT} - 1) \times 1000$$

$$\delta^{33}S_{CDT}\ (‰) = (R^{33}{}_{sample}/R^{33}{}_{CDT} - 1) \times 1000$$

where $R^{34} = {}^{34}S/{}^{32}S$, $R^{33} = {}^{33}S/{}^{32}S$ and the reference standard is Cañon Diablo troilite (CDT). A similar expression holds for $\delta^{36}S$; however, this value is rarely reported because the trace abundance of ^{36}S (0.02%) and mass spectrometric interferences (i.e., associated with the SF_6 technique) makes the measurement difficult. In fact, most studies have typically omitted the minor isotope ^{33}S (0.76% abundance) as well, expecting that there would be no new information conveyed by the measurement of $\delta^{33}S$. The reason for this expectation is that most physical, chemical, or biologic processes fractionate isotopes because of the relative mass differences of the isotopomers such that variations in $\delta^{33}S$ are correlated with those in $\delta^{34}S$. Because the mass difference between ^{33}S and ^{32}S is half of that between ^{34}S and ^{32}S, any effects in $\delta^{33}S$ would be about half those in $\delta^{34}S$. A more rigorous theoretical treatment leads to the definition of an equilibrium mass-dependent fractionation line given by $\delta^{33}S \approx 0.515 \times \delta^{34}S$ (Bigeleisen and Mayer, 1947; Hulston and Thode, 1965).

In the Earth's crust, $\delta^{34}S$ values generally exhibit a small range near 0‰ for igneous (0 ± 5‰) and hydrothermal (0 ± 10‰) rocks and ore bodies (Ohmoto and Rye, 1979; Ohmoto, 1986). Biologic (metabolic) processes typically result in much larger isotopic fractionations and bacterial sulfate reduction (Harrison and Thode, 1958) has been invoked to account for the >150‰ range in $\delta^{34}S$ from sulfates and sulfides in sedimentary rocks (Nielsen, 1979; Schidlowski et al., 1983). Phylogenetic inferences support the expectation that metabolic processing of sulfur (such as elemental sulfur reduction) is probably an ancient phenomenon (Stetter, 1996). As explained above, $\delta^{33}S$ values are not known for many samples because they were expected to strictly correlate with $\delta^{34}S$ along a mass-dependent fractionation line.

Recently, Farquhar and colleagues (2000)reported the occurrence of sedimentary sulfide and sulfate minerals in Archean rocks in which the minor sulfur isotopes do not lie on a mass-dependent fractionation line with other, younger terrestrial minerals. This so-called mass-independent fractionation (MIF) is characterized by nonzero values of $\Delta^{33}S$ and may be expressed as

$$\Delta^{33}S = \delta^{33}S - 1000 \times (1 + \delta^{34}S/1000)^{0.515}$$

For samples older than ~2450 Ma, $\Delta^{33}S$ was found to vary between −1.3 and +2.0‰, and samples younger than ~2000 Ma showed no resolvable $\Delta^{33}S$ anomalies within 0.1‰ (Farquhar et al., 2000). Analogous MIF anomalies in terrestrial samples have been previously seen in the oxygen isotopes of

---

[*] Author to whom correspondence should be addressed, at Department of Geological Sciences and Center for Astrobiology, University of Colorado, UCB 399, Boulder, CO 80309-0399 USA (mojzsis@colorado.edu).

O_3, CO, CO_2, N_2O, H_2O_2, and other species in the terrestrial atmosphere (Thiemens, 1999, and references therein) and in some massive sulfates derived from atmospheric deposition (Bao et al., 2000). Because it is thought that only certain unusual gas-phase chemical reactions are capable of producing anomalous three-isotope values on Earth, the discovery of the signal of this effect in geological materials has potentially important implications for understanding the chemical evolution of the atmosphere (Farquhar et al., 2000, 2001a; Pavlov and Kasting, 2002). The signature of this sulfur chemistry can be transferred from the atmosphere and incorporated into surface minerals, sediments, waters, and ices, probably via sulfate and elemental sulfur (e.g., S_8), or by dry deposition of H_2S, SO_2, etc., aerosols (Thiemens et al., 2001; Pavlov and Kasting, 2002). Subsequent isotopic exchange during chemical reactions in either the liquid or solid state results in mass-dependent isotopic fractionation, as well as possible mixing between different isotopic reservoirs. Thus, the MIF signature can potentially be preserved as a tracer of atmospheric sulfur at time of deposition, with its magnitude possibly diminished by mixing with sulfur from other sources with $\Delta^{33}S = 0‰$, such as volcanic emissions or dilution by the presently large oceanic sulfate reservoir.

The discovery of $\Delta^{33}S$ anomalies in Archean sediments (Farquhar et al., 2000) appears to open a new field in stable isotope geochemistry. However, the accuracy of the sulfur isotope measurements has been challenged because of possible analytical artifacts (Ohmoto et al., 2001). The analyses reported by Farquhar et al. (2000) were made on powdered whole rock or mineral separates of pyrite and barite, where oxidized and reduced sulfur was extracted by chemical procedures on bulk samples (Hulston and Thode, 1965; Forrest and Newman, 1977; Gao and Thiemens, 1993). The evolved H_2S from the extraction procedure was converted to Ag_2S and subsequently loaded into Ni reaction vessels with BrF_5 at 450°C to produce SF_6. After purification by gas chromatography, SF_6 was analyzed for ^{32}S, ^{33}S, ^{34}S, and ^{36}S by mass spectrometry. This procedure has been reproduced many times, which attests to the robustness of the technique (Farquhar et al., 2001b). A variant of the chemical extraction procedure utilizes a CO_2 laser and purified F_2 gas to fluorinate the same Ag_2S investigated by Farquhar et al. (2000). The laser fluorination method still relies on purification steps of SF_6 on a gas chromatograph (Rumble et al., 1993) or in a cold trap (Beaudoin et al., 1994) before the working gas is introduced to the mass spectrometer. Although the subsequent analyses (Farquhar et al., 2001b) apparently rebuff the criticisms raised by Ohmoto et al. (2001), because of the importance of these data, it makes sense to examine the issue by means of a completely independent approach.

Here we report analyses of $\delta^{33}S$ and $\delta^{34}S$ made by secondary ion mass spectrometry (SIMS) with simultaneous measurement of ^{32}S, ^{33}S, and ^{34}S using a multicollector detection system. The analyses are performed in situ on polished 2.54-cm round sections containing sulfide minerals, and thus there is no complex chemistry involved in the sample preparation that could possibly give rise to artifacts interpreted as MIF effects (cf. Ohmoto et al., 2001). Our technique has the additional advantage of being able to resolve $\Delta^{33}S$ anomalies at the ~25-μm scale, which permits investigation of the distribution of MIF sulfur isotope anomalies on an individual grain basis. Our aims were to first identify $\Delta^{33}S$ in ancient sulfides and to compare our results with the existing data set of $\Delta^{33}S$ in Precambrian rocks that have been used as evidence for changes in past atmospheric chemistry. We discuss the precision and accuracy of our measurements on sulfide standards and present ^{32}S, ^{33}S, and ^{34}S measurements on individual sulfides identified in petrographic thin sections prepared from a selection of 2.5 to 3.83 Ga rocks. Finally, we review the implications of our results for the evolution of atmospheric oxygen and sulfur biogeochemistry as well on the origin and nature of the oldest known sedimentary rocks.

2. ANALYTICAL TECHNIQUES

2.1. Description and Composition of Sulfide Standards

To make best use of the localized analysis capability of the ion microprobe, it is essential that samples be well characterized by microscopy and chemical analyses to preselect areas for study. Thus, all sulfide samples, including standards and unknowns, were first mapped by reflected light microscopy before electron microprobe analysis. Quantitative elemental analyses were carried out on the University of California–Los Angeles (UCLA) Cameca CAMEBAX electron microprobe (EPMA) by wavelength-dispersive (WDS) techniques following the usual procedures (Crowe and Vaughan, 1996); an accelerating potential of 15 kV, beam current of ~10 nA, and slightly defocused beam size of ~5 μm with a dwell time of 20 s (except for Co, which was 30 s) was used to prevent loss of S during analysis (Table 1).

2.1.1. *Pyrite (py)*

*2.1.1.1. Balmat pyrite (Bal).*The Balmat deposit is located in the Adirondack Mountains, New York, and occurs as massive sulfide hosted in Grenville-age marbles that were metamorphosed at peak conditions of 625°C and 6.5 kbar (Whelan et al., 1984). Balmat pyrite has occasional small inclusions of sphalerite (ZnS) that are readily identified during backscattered electron mapping and are specifically avoided during ion microprobe measurements. Aside from the rare ZnS inclusion, no other mineral phases are present, and WDS analysis indicates the sample is stoichiometric pyrite (FeS_2). The average $\delta^{34}S_{CDT}$ value for Balmat pyrite is $+15.1 \pm 0.2‰$ (Crowe and Vaughan, 1996).

*2.1.1.2. CAR 123 pyrite (123).*This pyrite standard was obtained from Dr. M. Chaussidon (CRPG-Nancy, France). The grains are subhedral masses of stoichiometric pyrite with $\delta^{34}S_{CDT} = +1.41 \pm 0.2‰$ (Chaussidon, 1988).

2.1.2. *Pyrrhotite (po)*

*2.1.2.1. Anderson pyrrhotite (AN).*This standard is from the Anderson Lake Mine, Manitoba, Canada. The sample is almost pure, crystalline pyrrhotite with very large subhedral to euhedral grains that are strongly magnetic. Analyses by WDS confirm a composition of $Fe_{0.87}S$; the average $\delta^{34}S_{CDT}$ value for Anderson pyrrhotite is $+1.4 \pm 0.3‰$ (Crowe and Vaughan, 1996).

2.1.2.2. LTB_1 pyrrhotite (LTB). This pyrrhotite standard was obtained from Dr. M. Chaussidon (CRPG-Nancy, France). The grains are small masses of stoichiometric pyrrhotite ($Fe_{1-x}S$; $x \approx 0.8$) with $\delta^{34}S_{CDT} = -0.32 \pm 0.2‰$ (Chaussidon, personal communication).

2.1.3. *Chalcopyrite (ch)*

*2.1.3.1. Trout Lake (TL22).*Trout Lake (TL22) is from a massive sulfide deposit located in Flin Flon, Manitoba, Canada. The deposit is part of a regionally metamorphosed greenschist-facies assemblage (Aggarwal and Nesbitt, 1987). Analyses by WDS confirm a composition of $CuFeS_2$; the average $\delta^{34}S_{CDT}$ value for Trout Lake chalcopyrite is $+0.3 \pm 0.3‰$ (Crowe and Vaughan, 1996).

2.1.3.2. OPM7151 (7151). This standard was obtained from Dr. M. Chaussidon (CRPG-Nancy, France). The grains occur as small anhedral masses of stoichiometric chalcopyrite with $\delta^{34}S_{CDT} = +2.29 \pm 0.2‰$ (Chaussidon, 1988).

Table 1. Electron microprobe analyses of sulfide standards used for ion microprobe multicollection.[a]

Grain_spot	Fe	Cu	Ni	Zn	Co	S	Total
7_1	62.9	0.16	0.07	0	0	37.0	100.13
7_2	63.8	0.00	0.10	0	0	35.3	99.20
7_3	63.3	0	0.07	0	0	36.6	99.97
7_4	63.6	0	0.04	0	0	36.7	100.34
4_2	60.4	0	0.10	0	0	39.2	99.70
4_3	59.6	0	0.03	0	0	40.2	99.83
4_1	59.3	0	0	0	0	39.9	99.20
5_1	31.2	0	35.2	0	0.66	33.5	100.56
5_2	30.8	0	34.8	0	0.54	33.4	99.54
3_6	59.8	0	0.38	0	0	39.4	99.58
3_7	30.7	0	35.2	0	0.69	32.8	99.39
3_8	59.4	0	0.42	0	0	39.5	99.32
6_4	30.5	34.1	0.01	0	0	34.6	99.21
6_5	39.7	23.5	0.07	0	0	35.0	98.27
6_6	30.1	34.2	0.09	0	0	34.1	98.49
6_1	30.2	34.3	0.03	0	0	34.1	98.63
6_2[b]	8.09	3.6	0.03	55.4	0	33.2	100.32
6_3	30.2	34.2	0.03	0	0	34.4	98.83
3_3	30.0	34.1	0	0	0	34.3	98.40
3_4[b]	30.6	34.5	0.14	0.26	0	34.7	100.20
3_5	29.7	34.3	0.08	0	0	34.3	98.38
3_1	30.4	34.3	0	0	0	34.4	99.10
3_2	30.3	34.3	0.06	0	0	34.9	99.56
1_3	47.2	0	0	0	0	52.7	99.90
1_4	47.1	0	0.07	0	0	53.6	100.77
1_1	47.7	0	0	0	0	53.5	101.20
1_2	46.6	0	0.03	0	0	53.9	100.53
2_3	46.7	0	0.13	0	0	53.6	100.43
2_1	47.3	0	0.05	0	0	53.4	100.75
2_2	47.4	0	0	0	0	53.1	100.50

[a] Nomenclature is standard + EPMA spot number; 1 = *CAR123* pyrite (py), 2 = *Balmat* (py), 3 = *Trout Lake* chalcopyrite (ch), 4 = *Anderson* pyrrhotite (po), *5 = LTB* (po), 6 = *7151* (po), 7 = *CDT* (tr); 0 = not detected. Data presented in terms of weight percentage. Detection limits for the counting statistics were 0.1 (2σ) for Zn, Cu, and Co; $\leq$0.01 (2σ) for Ni.

[b] Sphalerite inclusion.

2.1.4. *Troilite (tr)*

2.1.4.1. Cañon Diablo (CDT). Troilite (FeS) in the iron meteorite Cañon Diablo was adopted as the isotope scale reference for sulfur and is defined as $^{34}S/^{32}S = 4.50045 \times 10^{-2}$, $^{33}S/^{32}S = 7.9560 \times 10^{-3}$, and $^{34}S/^{33}S = 5.6567$ (Ault and Jensen, 1962; cf. Ding et al., 2001). The terrestrial mass-dependent isotope fractionation line in three-isotope space ($\delta^{33}S/\delta^{34}S$) is defined as intercepting 0.00‰ at $(^{33}S/^{32}S)/(^{34}S/^{32}S)_{CDT}$ with a slope of 0.5155 (Hulston and Thode, 1965). We recognize that, as a standard, CDT is problematic in displaying a range in $\delta^{34}S$ values of ~0.4‰ (Beaudoin et al., 1994). Additionally, the absolute ($^{34}S/^{32}S$) ratio of CDT probably requires substantial revision (Ding et al., 2001). However, we choose to report our data relative to CDT because of its historical importance in sulfur isotope studies. Note that because we report δ-values relative to CDT, the absolute isotopic composition of its sulfur has no significant effect on our data. Similarly, uncertainties in the composition of CDT (or any of the other standards employed in this study) are small compared with analytical errors and thus do not compromise our determination of the $\delta^{33}S/\delta^{34}S$ mass fractionation line in our present measurement protocol (Greenwood et al., 2000). Our standard occurs as individual troilite blebs extracted from the Cañon Diablo meteorite (McEwing et al., 1983); the average composition of CDT $\delta^{34}S \equiv 0$‰.

2.2. Sample Preparation Methods

To make the ion microprobe standards mount used in this study (GM3), individual ~1-mm-diameter standard grains, each freshly broken from the same larger grain, were placed onto adhesive tape under a binocular microscope. The enclosing 2.54-cm-diameter mold was then cast with epoxy, cured, removed from its mold, and hand polished in diamond paste on a felt lap to a 1-μm diamond grit size and subsequently polished with 0.25-μm alumina. Care was taken to avoid oxidation and pitting of the sulfides during the polishing process. All samples were ultrasonically cleaned and then coated with 100 Å of gold before SIMS microanalysis to ensure conductivity across the sample surface.

Replicate mass spectrometric analyses were performed on each standard grain to verify $\delta^{33}S$ and $\delta^{34}S$ homogeneity at the subgrain scale and to correct for mineral-specific instrumental mass fractionation (IMF) effects. At the scale of ion microprobe measurements, where sample domains can be on the order of several tens of micrometers, the standards exhibit some variability, but on average appear to be homogeneous in $\Delta^{33}S$ within the precision of individual analyses. The variability in $\delta^{34}S$ in individual sulfide standards (including CDT; Beaudoin et al., 1994) can be attributed to sample heterogeneity in $\delta^{34}S$ but not in $\Delta^{33}S$, which was the first-order purpose of the standards. A critical aspect was to evaluate the accuracy of in situ multicollector SIMS data on sulfides. A previous ion microprobe multi-isotope sulfur study (Greenwood et al., 2000) relied on the analysis of intercomparison pyrites (Balmat and CAR123) to convert raw machine data—that is, $\delta^{34}S_{1270}$, a number measured before mass-bias corrections (Riciputi et al., 1998), to values relative to CDT. We extend this approach to intercomparison of our pyrrhotite standards (Anderson, LTB and OPM7151). Furthermore, after mass bias corrections are applied, we compare the SIMS value with the $\delta^{34}S$ values of each standard as measured by conventional methods. Separate small standard mounts were prepared in the same manner as described above and mounted alongside the unknowns in the sample holder; these served as internal calibrants for both ease of regular standardization and to monitor possible changes in acquisition conditions from potential instrument and/or geometric effects of the use of a different sample holder for the standards and unknowns.

2.3. Ion Microprobe Multicollector Analysis

All sulfides analyzed in this study were measured for their sulfur isotopes with the UCLA Cameca ims 1270 high-resolution ion microprobe in multicollector mode with a 2.9-nA, 20-keV Cs^+ primary ion beam focused to a ~25-μm spot. This method simultaneously measures ^{32}S, ^{33}S, and ^{34}S on adjacent detectors. Before analysis, samples were sputtered for 500 s to minimize transient isotopic fractionation effects due to preferential sputtering (which could affect mass fractionation only). Analyses then comprised 15 cycles of 10-s measurements, including spot-to-spot setup time. Total time per analysis was ~12 min. Negative secondary ions with initial energies in the range 0 to 25 eV were analyzed, and a normal-incidence electron flood gun was used to neutralize positive charge buildup in the analysis area. Faraday cups were used to collect $^{32}S^-$, $^{33}S^-$, and $^{34}S^-$ beams and signals amplified by Finnegan electrometers housed in a temperature-controlled evacuated chamber. Secondary beam currents are quoted here in equivalent counts per second (cps). A mass resolving power of 4000 was sufficient to maintain the $^{32}SH^-$ contribution to the $^{33}S^-$ peak to <10 ppm. Count rates on $^{33}S^-$ were in the range 7.3 to 31.0 × 10^6 cps with corresponding count rates of $^{32}S^-$ and $^{34}S^-$ in the range 2 to 3 × 10^9 cps and 100 to 500 × 10^6 cps, respectively. At these count rates, the reproducibility of the baseline current in the Faraday cup amplifiers becomes a limiting factor on the precision and accuracy of $\Delta^{33}S$ determinations at the level of ~0.1‰. However, no correlation between $\Delta^{33}S$ and count rate of $^{33}S^-$ was observed, indicating that baseline corrections are accurate (Fig. 1).

2.4. IMF Correction

It is known that isotopic ratios measured by SIMS deviate from the true isotopic ratios of the sample in a systematic way as a function of isotopic mass (e.g., Ireland, 1995; Riciputi et al., 1998). The IMF effect is due to the isotopic fractionation in the ionization process during sputtering, fractionation experienced by the secondary ions during their transport from the sample surface to the detectors and the possible mass (i.e., velocity)-dependent response of the detectors. For practical pur-

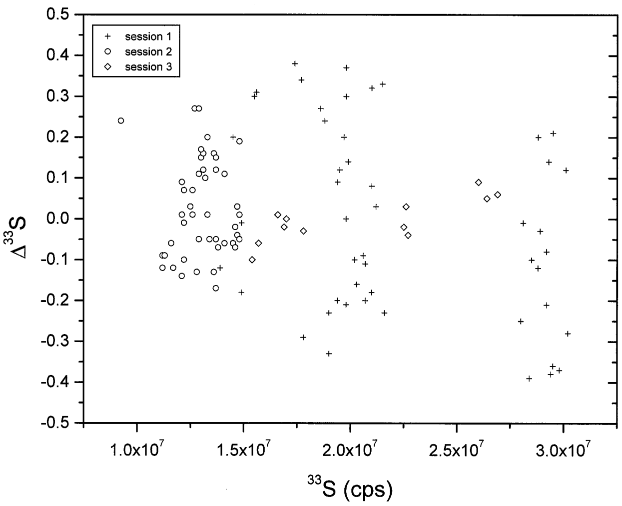

Fig. 1. Plot of $\Delta^{33}S$ vs. ^{33}S (cps; counts per second) of standard sulfide minerals measured by multicollector ion microprobe. The total range found in $\Delta^{33}S$ is -0.39 ± 0.08 to $+0.38 \pm 0.07$‰, defined mostly in analysis session 1. We conclude that there is no correlation between count rate and $\Delta^{33}S$ value in our analysis.

poses of SIMS analysis, IMF can be corrected for by external and internal calibration against standards under the same instrumental conditions (Zinner, 1989; Ireland, 1995; Riciputi, 1996; Riciputi et al., 1998). We used the weighted mean of the measurements made on standards of the same sulfide phases as the unknowns and monitored IMF separately for each analysis session. The measured $\Delta^{34}S_{IMF}$ used to correct the standards data are listed in Table 2; these data assume the composition for CDT (Ault and Jensen, 1962).

3. APPLICATIONS AND RESULTS

3.1. Standards and Establishment of the Mass Fractionation Line for Three Sulfur Isotopes

Table 3. $(^{33}S/^{32}S)_{CDT}$ and $(^{34}S/^{33}S)_{CDT}$ reference ratios established by individual analysis session.

Analysis session	$(^{34}S/^{32}S)$[a]	$(^{33}S/^{32}S)_{measured}$	$(^{34}S/^{33}S)$
05-23 to 05-25-00 (1)	4.50045E-02	7.9560E-03	5.6567
01-04 to 01-06-01 (2)	4.50045E-02	7.9573E-03	5.6558
04-21-01 (3)	4.50045E-02	7.9590E-03	5.6545

[a] $(^{34}S/^{32}S)_{CDT} = 0.045005$ by definition.

The mass fractionation line on a three-isotope plot was determined by 120 separate analyses of sulfide standards over three separate analysis sessions; the results of these analyses are presented in Table 3. The measured $(^{33}S/^{32}S)$ reference ratios were corrected for IMF assuming an exponential mass fractionation law (Zinner, 1989). The slope of the mass fractionation line established by using these data on a plot of $\delta^{33}S$ against $\delta^{34}S$ is 0.515, and hence, we define $\Delta^{33}S = \delta^{33}S - 1000 \times (1 + \delta^{34}S/1000)^{0.515}$. Such a slope is within the expected range of values for mass-dependent fractionation by equilibrium or kinetic processes (Hulston and Thode, 1965; Young et al., 2002).

The measured ranges in $\Delta^{33}S$ for the sulfide standards were different for each of the three analytical sessions, with the scatter being progressively reduced as the measurement technique improved with time. In the first session, the extreme values in $\Delta^{33}S$ ranged from -0.39 ± 0.084 to $+0.38 \pm 0.070$‰, whereas in session 2, corresponding values were -0.17 ± 0.064 to $+0.37 \pm 0.078$‰, and in session 3, the total range measured on individual spots ranged from -0.10 ± 0.050 to $+0.09 \pm 0.054$‰ (Fig. 2). The stated uncertainties on these standard measurements reflect only internal reproducibility, and there are additional sources of error associated with instrument tuning and detector performance (particularly stability of the baseline). With the exception of the Trout Lake chalcopyrite, for which $\Delta^{33}S = -0.26$‰, the remaining six standard materials all display mean $\Delta^{33}S$ values within 0.065‰ of a common mass-dependent fractionation line (Table 2). Although there may exist minor sulfur isotope anomalies among some of these "standard" materials, this level of reproducibility suggests that we can clearly resolve anomalous sulfur (i.e., $\Delta^{33}S \neq 0$) at the (2σ) level of 0.3‰ in the first analytical

Table 2. Instrumental mass fractionation ($\Delta^{34}S_{IMF}$) by sulfide phase.

Group name	Phase	$(^{34}S/^{32}S)$[a]	$\delta^{14}S_{CDT}$ (‰)	$\Delta^{34}S_{IMF}$ (‰)	$\pm 1\sigma$ (‰)	$\Delta^{33}S$[b] (‰)	$\pm 2\sigma_{STD}$ (‰)
05-23 to 05-25-00 (session 1)							
CAR123	py	0.045068	1.41	−17.36	0.20	0.064	0.044
TL22	ch	0.045018	0.30	−16.99	0.36	−0.257	0.063
LTB	po	0.045019	−0.32	−22.69	0.59	−0.021	0.154
AN	po	0.045068	1.40	−21.44	0.11	0.020	0.044
CDT	tr	0.045005	0.00	−23.55	0.17	−0.029	0.020
01-04 to 01-06-01 (session 2)							
Bal	py	0.045684	15.10	−17.13	0.13	0.014	0.023
CAR123	py	0.045068	1.41	−18.24	0.27	0.064	0.044
AN	po	0.045068	1.40	−21.89	0.30	0.020	0.044
CDT	tr	0.045005	0.00	−25.47	0.32	−0.029	0.020
04-21-01 (session 3)							
Bal	py	0.045684	15.10	−17.65	0.04	0.014	0.023
LTB	po	0.044990	−0.32	−23.04	0.02	−0.021	0.154
OPM7151	ch	0.045108	2.29	−21.01	0.06	0.065	0.012
CDT	tr	0.045005	0.00	−24.96	0.27	−0.029	0.020

[a] Measured ratio, uncorrected for IMF.
[b] Mean $\Delta^{33}S$ values over all standard sessions (Table 4).

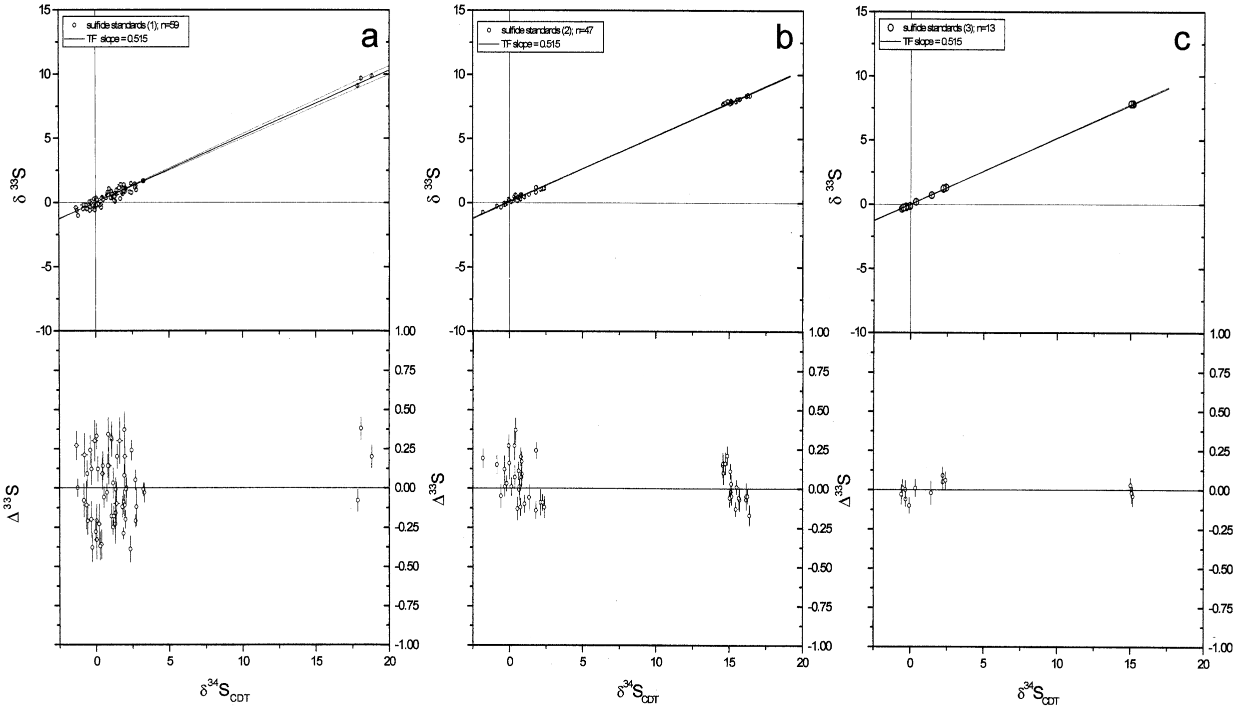

Fig. 2. Plots of $\delta^{33}S$ and $\Delta^{33}S$ vs. $\delta^{34}S$ for separate analysis sessions by ion microprobe multicollection. The slope $m = 0.515$ line in each session (a–c) is the best fit to our data for terrestrial sulfides and CDT standards. (a) Analysis session 1 ($n = 59$) had the largest scatter in $\delta^{33}S/\delta^{34}S$ and is responsible for the maximum total range in $\Delta^{33}S$ reported for our standards (Fig. 1). (b) Analysis session 2 ($n = 47$) and (c) analysis session 3 ($n = 13$) had the tightest bounds around the 0.515 regression line defining mass fractionation (see text). Uncertainties are reported at the 2σ level, and the upper and lower 95% confidence limits to the regression are depicted.

session, and 0.2‰ for the remaining two sessions. In considering the possibility of sample heterogeneity, we report overall uncertainties for single spot analyses by adding internal reproducibility in quadrature with this estimate of the external reproducibility on all standards, again, neglecting Trout Lake chalcopyrite, which might well be anomalous at close to our detection limit (Table 4).

3.2. Archean Sulfide Samples

Both pyrite and pyrrhotite from a range of rock types, ages, and metamorphic grade were analyzed to test the efficacy of the multicollector SIMS system and to evaluate the degree of $\delta^{34}S$, $\delta^{33}S$, and thereby $\Delta^{33}S$, in samples from several Archean and Proterozoic banded iron formations (BIF), a metamorphosed chert, garnet–biotite schist (ferruginous metapelite) and an Fe-rich quartzite. The results are discussed in the following sections and data from all analyses are reported in Table 5.

Freshly broken and unweathered 1- to 4-kg samples of the selected rocks were split manually and cut into chips by diamond saws. Samples of each rock used in this study contained visible (albeit generally tiny) sulfides; thin sections of each were prepared by standard petrographic techniques. The occurrences of sulfides in each sample were mapped and characterized by reflected light microscopy and WDS-EPMA following the procedures described above. In some cases where only minute grains were present near the edge of the sample, the thin sections were then divided with a small petrographic saw around the S-rich regions, placed face-down on double-sided tape with several sulfide standards, cast in epoxy, and polished on 0.25-μm alumina in alcohol. Before ion microprobe analysis, all samples were ultrasonically cleaned in ultrapure water and ethanol before coating with ~100 Å of Au with a sputter coater.

3.2.1. Brockman Iron Formation, Hamersley Basin, Western Australia (BH1), ~2.47 Ga

A sample of late Archean BIF was examined (Brockman iron formation, Hamersley Group, Western Australia). This is a finely banded BIF that has been long studied and is part of a widespread deposit in the Hamersley Basin (Trendall and Morris, 1983). Numerous workers have used sulfur isotope ratio measurements to elucidate temperature, sulfur sources, fluid histories and biologic effects from BIF in the Hamersley Group (Strauss and Moore, 1992). Recent research has been focused on $\delta^{34}S$ and $\Delta^{33}S$ values for sulfides derived from these and other late Archean to early Proterozoic deposits, which may represent reduction of seawater sulfate preserving MIF effects in pyrite (Farquhar et al., 2000). Sulfides in this sample are restricted to thin bands of pyrite parallel to the sense of sedimentary microbanding (Fig. 3). A small sample chip with visible sulfides was used in the preparation of a thin section. Ion microprobe $\delta^{33}S/\delta^{34}S$ measurements of Hamersley BIF *BH1*

Table 4. Sulfur isotopic compositions of standard minerals measured by ion microprobe multicollection.

Grain_spot	$^{34}S/^{32}S$	$\pm 1\sigma$	$^{33}S/^{32}S$	$\pm 1\sigma$	$\delta^{34}S_{CDT}$[a] (‰)	$\pm 2\sigma$[b] (‰)	$\delta^{33}S_{CDT}$[c] (‰)	$\pm 2\sigma$ (‰)	$\Delta^{33}S$[d] (‰)	$\pm 2\sigma$[e] (‰)
Pyrite (py)										
05-23-00 CAR123										
GM3_123b_5	4.50976E-02	1.59E-06	7.96E-03	1.967E-7	2.07	0.070	1.06	0.050	0.00	0.062
05-24-00 CAR123										
BH1_123_5	4.50564E-02	9.11E-07	7.96E-03	1.76E-07	1.15	0.040	0.34	0.044	−0.25	0.048
BH1_123b_1	4.50675E-02	4.68E-06	7.96E-03	3.53E-07	1.40	0.208	0.61	0.088	−0.10	0.138
BH1_123b_2	4.51099E-02	1.16E-06	7.96E-03	3.19E-07	2.34	0.052	0.82	0.080	−0.39	0.084
BH1_123_8	4.50421E-02	3.20E-06	7.96E-03	3.15E-07	0.84	0.142	0.77	0.080	0.34	0.108
BH1_123_9	4.50254E-02	2.51E-06	7.96E-03	2.72E-07	0.46	0.112	0.38	0.068	0.14	0.090
BH1_123_10	4.50213E-02	2.88E-06	7.95E-03	2.60E-07	0.37	0.128	−0.17	0.066	−0.36	0.092
05-25-00 Balmat										
GM3_Bal1_1	4.58182E-02	1.15E-06	8.03E-03	2.63E-07	18.08	0.050	9.67	0.066	0.38	0.070
GM3_Bal1_2	4.58511E-02	2.26E-06	8.03E-03	2.00E-07	18.81	0.098	9.86	0.050	0.20	0.070
GM3_Bal1_3	4.58078E-02	2.48E-06	8.03E-03	1.67E-07	17.85	0.108	9.09	0.042	−0.08	0.070
05-25-00 CAR123										
PB6b_123_1	4.51527E-02	1.29E-06	7.97E-03	2.08E-07	3.29	0.056	1.66	0.052	−0.03	0.060
PB6b_123_2	4.51284E-02	2.44E-06	7.97E-03	4.22E-07	2.75	0.108	1.29	0.106	−0.12	0.120
PB6b_123_3	4.51503E-02	6.17E-07	7.97E-03	1.57E-07	3.24	0.028	1.66	0.040	−0.01	0.042
PB6b_123_6	4.51254E-02	2.08E-06	7.97E-03	1.70E-07	2.69	0.092	1.43	0.042	0.05	0.064
PB6b_123_7	4.50437E-02	4.10E-06	7.96E-03	2.72E-07	0.87	0.182	0.58	0.068	0.14	0.116
PB6b_123_8	4.50824E-02	4.61E-06	7.97E-03	2.73E-07	1.73	0.204	1.39	0.068	0.50	0.126
01-04-01 Balmat										
GM3_Bal1_1	4.56597E-02	2.89E-07	8.02E-03	3.10E-07	14.56	0.012	7.73	0.078	0.15	0.078
GM3_Bal1_2	4.56606E-02	5.72E-07	8.02E-03	2.02E-07	14.58	0.026	7.75	0.050	0.16	0.056
GM3_Bal1_3	4.56616E-02	5.50E-07	8.02E-03	2.71E-07	14.60	0.024	7.71	0.068	0.10	0.072
GM3_Bal1_4	4.56674E-02	4.34E-07	8.02E-03	2.71E-07	14.73	0.020	7.83	0.068	0.16	0.070
GM3_Bal1_5	4.56831E-02	5.21E-07	8.02E-03	1.67E-07	15.08	0.022	7.97	0.042	0.11	0.048
GM3_Bal1_6	4.56733E-02	4.21E-07	8.02E-03	2.22E-07	14.86	0.018	7.95	0.056	0.21	0.058
01-04-01 CAR123										
GM3_123_1	4.50023E-02	5.56E-07	7.96E-03	2.58E-07	−0.05	0.024	0.25	0.064	0.27	0.070
GM3_123_2	4.50205E-02	5.34E-07	7.96E-03	3.41E-07	0.35	0.024	0.45	0.086	0.27	0.088
GM3_123_3	4.50232E-02	6.73E-07	7.96E-03	2.85E-07	0.42	0.030	0.59	0.072	0.37	0.078
01-05-01 Balmat										
GM3_Bal1_1	4.5683E-02	4.78E-07	8.02E-03	1.62E-07	15.09	0.020	7.82	0.040	−0.04	0.046
GM3_Bal1_2	4.5686E-02	5.93E-07	8.02E-03	1.86E-07	15.15	0.026	7.84	0.046	−0.05	0.054
GM3_Bal1_3	4.5701E-02	6.02E-07	8.02E-03	1.39E-07	15.49	0.026	8.07	0.034	0.01	0.044
GM3_Bal1_4	4.5684E-02	4.43E-07	8.02E-03	1.42E-07	15.10	0.020	7.85	0.036	−0.02	0.040
GM3_Bal1_5	4.5685E-02	4.70E-07	8.02E-03	2.21E-07	15.13	0.020	7.91	0.056	0.03	0.058
GM3_Bal1_6	4.5681E-02	4.40E-07	8.02E-03	2.23E-07	15.03	0.020	7.77	0.056	−0.06	0.058
01-05-01 CAR123										
GM3_123_1	4.50327E-02	4.83E-07	7.96E-03	2.05E-07	0.63	0.022	0.44	0.052	0.11	0.056
GM3_123_2	4.50862E-02	7.02E-07	7.97E-03	1.66E-07	1.82	0.032	1.19	0.042	0.24	0.052
GM3_123_3	4.49663E-02	4.56E-07	7.96E-03	2.15E-07	−0.85	0.020	−0.29	0.054	0.15	0.058
GM3_123_4	4.50425E-02	6.01E-07	7.96E-03	2.26E-07	0.84	0.026	0.61	0.056	0.17	0.062
GM3_123_5	4.50403E-02	4.36E-07	7.96E-03	2.21E-07	0.79	0.020	0.61	0.056	0.20	0.058
01-06-01 Balmat										
GM3_Bal1_1	4.57414E-02	6.12E-07	8.02E-03	2.31E-07	16.37	0.026	8.36	0.058	−0.17	0.064
GM3_Bal1_2	4.57111E-02	6.53E-07	8.02E-03	2.68E-07	15.70	0.028	8.11	0.066	−0.07	0.072
GM3_Bal1_3	4.56995E-02	4.95E-07	8.02E-03	1.59E-07	15.44	0.022	7.91	0.040	−0.13	0.046
GM3_Bal1_4	4.57092E-02	4.85E-07	8.02E-03	2.80E-07	15.66	0.022	8.09	0.070	−0.06	0.072
GM3_Bal1_5	4.57307E-02	4.94E-07	8.02E-03	2.27E-07	16.14	0.022	8.33	0.056	−0.07	0.060
GM3_Bal1_6	4.57315E-02	9.09E-07	8.02E-03	2.95E-07	16.15	0.040	8.37	0.074	−0.05	0.084
GM3_Bal1_7	4.57354E-02	5.26E-07	8.02E-03	1.55E-07	16.24	0.022	8.41	0.038	−0.05	0.044
04-21-01 Balmat										
GM3_Bal1_1	4.56872E-02	4.92E-07	8.02E-03	2.34E-07	15.17	0.022	7.83	0.058	−0.04	0.062
GM3_Bal1_2	4.56846E-02	6.33E-07	8.02E-03	2.25E-07	15.11	0.028	7.82	0.056	−0.02	0.062
GM3_Bal1_3	4.56804E-02	6.40E-07	8.02E-03	1.42E-07	15.02	0.028	7.82	0.036	0.03	0.046
Chalcopyrite (ch)										
05-23-00 Trout Lake										
GM3_TLb_2	4.50884E-02	8.06E-07	7.96E-03	1.22E-07	1.86	0.036	0.67	0.030	−0.29	0.036
05-24-00 Trout Lake										
BH1_TL_1	4.49688E-02	5.37E-06	7.95E-03	2.49E-07	−0.79	0.238	−0.19	0.062	0.21	0.138
BH1_TL_2	4.50033E-02	1.58E-06	7.95E-03	1.55E-07	−0.03	0.070	−0.29	0.038	−0.28	0.054
BH1_TL_3	4.49903E-02	3.04E-06	7.96E-03	2.84E-07	−0.31	0.136	−0.04	0.072	0.12	0.100
05-25-00 Trout Lake										
PB6b_TL_1	4.49930E-02	2.08E-06	7.95E-03	3.14E-07	−0.26	0.092	−0.51	0.078	−0.38	0.092
PB6b_TL_2	4.50173E-02	1.71E-06	7.95E-03	3.20E-07	0.28	0.076	−0.23	0.080	−0.37	0.090

Table 4. (Continued)

Grain_spot	$^{34}S/^{32}S$	$\pm 1\sigma$	$^{33}S/^{32}S$	$\pm 1\sigma$	$\delta^{34}S_{CDT}$[a] (‰)	$\pm 2\sigma$[b] (‰)	$\delta^{33}S_{CDT}$[c] (‰)	$\pm 2\sigma$ (‰)	$\Delta^{33}S$[d] (‰)	$\pm 2\sigma$[e] (‰)
Pyrrhotite (po)										
05-23-00 Anderson										
GM3_Ana_6	4.50849E-02	9.28E-07	7.96E-03	2.52E-07	1.79	0.042	0.79	0.064	−0.12	0.066
GM3_Ana_7	4.50694E-02	1.53E-06	7.96E-03	2.71E-07	1.44	0.068	0.94	0.068	0.20	0.076
GM3_Ana_8	4.50649E-02	1.43E-06	7.96E-03	2.77E-07	1.34	0.064	0.68	0.070	−0.01	0.076
PB6a_An_1	4.50517E-02	1.49E-06	7.96E-03	2.91E-07	1.05	0.066	0.36	0.074	−0.18	0.080
PB6a_An_2	4.50004E-02	4.86E-06	7.96E-03	2.65E-07	−0.09	0.216	0.26	0.066	0.30	0.130
PB6a_An_3	4.50526E-02	2.33E-06	7.96E-03	3.81E-07	1.07	0.104	0.86	0.096	0.31	0.110
05-24-00 Anderson										
BH1_An_6	4.50567E-02	2.18E-06	7.96E-03	3.25E-07	1.16	0.096	0.63	0.082	0.03	0.096
BH1_An_7	4.50061E-02	2.74E-06	7.96E-03	2.02E-07	0.04	0.122	0.34	0.050	0.33	0.080
BH1_An_8	4.50518E-02	2.38E-06	7.96E-03	1.78E-07	1.05	0.106	0.86	0.044	0.32	0.070
BH1_An_9	4.50138E-02	3.50E-06	7.96E-03	3.83E-07	0.21	0.156	−0.12	0.096	−0.23	0.126
05-25-00 Anderson										
GM3_Ana_5	4.50645E-02	2.14E-06	7.96E-03	3.81E-07	1.33	0.094	0.52	0.096	−0.16	0.108
GM3_Ana_8	4.50932E-02	3.33E-06	7.97E-03	3.29E-07	1.97	0.148	1.21	0.082	0.20	0.112
PB6b_An_5	4.50970E-02	2.47E-06	7.96E-03	2.92E-07	2.05	0.110	1.04	0.074	−0.01	0.092
PB6b_An_6	4.50893E-02	1.41E-06	7.96E-03	2.75E-07	1.88	0.062	0.87	0.070	−0.09	0.076
PB6b_An_1	4.50947E-02	5.31E-07	7.96E-03	2.27E-07	2.01	0.024	0.83	0.058	−0.20	0.058
PB6b_An_2	4.50911E-02	5.38E-07	7.96E-03	2.78E-07	1.92	0.024	1.07	0.070	0.08	0.070
05-25-00 Anderson (continued)										
PB6b_An_3	4.50585E-02	4.98E-07	7.96E-03	2.48E-07	1.20	0.022	0.44	0.062	−0.18	0.064
PB6b_An_4	4.50917E-02	6.41E-07	7.96E-03	2.62E-07	1.94	0.028	0.89	0.066	−0.11	0.068
PB6b_An_7	4.50921E-02	2.65E-06	7.97E-03	3.83E-07	1.95	0.118	1.37	0.096	0.37	0.114
PB6b_An_8	4.50772E-02	4.77E-06	7.96E-03	3.91E-07	1.62	0.212	1.13	0.098	0.30	0.146
PB6b_An_9	4.50636E-02	2.13E_06	7.96E-03	4.50E-07	1.31	0.094	0.44	0.114	−0.23	0.124
PB6b_An_10	4.50059E-02	3.51E-06	7.95E-03	3.74E-07	0.03	0.156	−0.32	0.094	−0.33	0.124
PB6b_An_11	4.51135E-02	1.02E-06	7.97E-03	2.36E-07	2.42	0.046	1.48	0.060	0.24	0.064
05-25-00 LTB										
GM3_LTB_1	4.50061E-02	1.47E-06	7.95E-03	3.94E-07	0.04	0.066	−0.19	0.100	−0.21	0.104
GM3_LTB_2	4.49880E-02	1.86E-06	7.95E-03	3.70E-07	−0.37	0.082	−0.63	0.092	−0.44	0.102
GM3_LTB_3	4.49447E-02	3.36E-06	7.95E-03	2.02E-07	1.33	0.150	−0.41	0.050	0.27	0.092
GM3_LTB_4	4.50101E-02	2.19E-06	7.96E-03	2.39E-07	0.12	0.098	0.19	0.060	0.12	0.078
01-05-01 Anderson										
GM3_Ana_1	4.50348E-02	6.44E-07	7.96E-03	2.38E-07	0.67	0.028	0.34	0.060	−0.01	0.066
GM3_Ana_2	4.50353E-02	4.94E-07	7.96E-03	1.84E-07	0.69	0.022	0.37	0.046	0.01	0.052
GM3_Ana_3	4.50415E-02	6.36E-07	7.96E-03	2.14E-07	0.82	0.028	0.50	0.054	0.07	0.060
GM3_Ana_4	4.50427E-02	4.97E-07	7.96E-03	2.58E-07	0.85	0.022	0.53	0.064	0.09	0.068
01-06-01 Anderson										
GM3_Ana_1	4.51003E-02	5.99E-07	7.97E-03	3.10E-07	2.13	0.026	1.02	0.078	−0.09	0.082
GM3_Ana_2	4.51066E-02	4.97E-07	7.97E-03	1.75E-07	2.27	0.022	1.09	0.044	−0.09	0.050
GM3_Ana_3	4.51114E-02	4.39E-07	7.97E-03	2.50E-07	2.38	0.020	1.12	0.062	−0.12	0.066
04-21-01 7151										
7151_1	4.51050E-02	3.56E-07	7.97E-03	1.72E-07	2.23	0.016	1.2	0.044	0.05	0.046
7151_2	4.51131E-02	3.64E-07	7.97E-03	2.04E-07	2.41	0.016	1.31	0.052	0.06	0.054
7151_3	4.51046E-02	5.19E-07	7.97E-03	1.98E-07	2.22	0.024	1.24	0.050	0.09	0.054
Cañon Diablo troilite (CDT)										
05-25-00 Cañon Diablo										
PB6a_CDT_1	4.49769E-02	1.48E-06	7.95E-03	3.08E-07	−0.61	0.066	−0.22	0.078	0.09	0.084
PB6b_CDT_1	4.49868E-02	2.91E-06	7.96E-03	2.61E-07	−0.39	0.130	0.04	0.066	0.24	0.094
PB6b_CDT_2	4.49750E-02	4.77E-06	7.95E-03	4.17E-07	−0.66	0.212	−0.45	0.104	−0.11	0.152
PB6b_CDT_3	4.49478E-02	1.68E-06	7.95E-03	1.58E-07	−1.26	0.074	−0.64	0.040	0.00	0.056
GM3_CDTb_2	4.50411E-02	1.56E-06	7.96E-03	2.54E-07	0.81	0.070	0.56	0.064	0.14	0.074
GM3_CDTb_3	4.50239E-02	3.50E-06	7.96E-03	2.44E-07	0.43	0.156	0.31	0.062	0.09	0.100
GM3_CDTb_4	4.49894E-02	4.15E-06	7.95E-03	2.55E-07	−0.33	0.184	−0.37	0.064	−0.20	0.114
BH1_CDT_1	4.49671E-02	2.97E-06	7.95E-03	3.25E-07	−0.83	0.132	−0.50	0.082	−0.08	0.106
BH1_CDT_2	4.49784E-02	2.80E-06	7.95E-03	2.40E-07	−0.58	0.124	−0.51	0.060	−0.21	0.088
PB6b_CDT_7	4.50284E-02	1.22E-06	7.96E-03	2.38E-07	0.53	0.054	0.21	0.060	−0.06	0.066
PB6b_CDT_8	4.50379E-02	7.62E-07	7.96E-03	2.12E-07	0.74	0.034	0.35	0.054	−0.03	0.056
PB6b_CDT_9	4.49514E-02	1.50E-06	7.95E-03	2.29E-07	−1.18	0.066	−1.02	0.058	−0.41	0.068
01-04-01 Cañon Diablo										
GM3_CDT_2	4.50211E-02	6.91E-07	7.96E-03	2.71E-07	0.37	0.030	0.26	0.068	0.07	0.074
GM3_CDT_3	4.49958E-02	5.97E-07	7.96E-03	1.65E-07	−0.19	0.027	−0.07	0.042	0.03	0.050
GM3_CDT_4	4.50042E-02	1.68E-06	7.96E-03	2.83E-07	−0.01	0.074	0.15	0.072	0.16	0.102
GM3_CDT_5	4.49896E-02	5.93E-07	7.96E-03	3.27E-07	−0.33	0.026	−0.05	0.082	0.12	0.086
GM3_CDT_6	4.49230E-02	5.93E-07	7.95E-03	2.18E-07	−1.81	0.026	−0.75	0.054	0.19	0.060

Table 4. (Continued)

Grain_spot	$^{34}S/^{32}S$	$\pm 1\sigma$	$^{33}S/^{32}S$	$\pm 1\sigma$	$\delta^{34}S_{CDT}$[a] (‰)	$\pm 2\sigma$[b] (‰)	$\delta^{33}S_{CDT}$[c] (‰)	$\pm 2\sigma$ (‰)	$\Delta^{33}S$[d] (‰)	$\pm 2\sigma$[e] (‰)
Cañon Diablo troilite (CDT)—(continued)										
01-05-01 Cañon Diablo										
GM3_CDT_1	4.49782E-02	5.77E-07	7.95E-03	2.72E-07	−0.58	0.026	−0.35	0.068	−0.05	0.074
GM3_CDT_2	4.50104E-02	5.20E-07	7.96E-03	2.08E-07	0.13	0.024	0.08	0.052	0.01	0.058
GM3_CDT_3	4.49900E-02	6.62E-07	7.96E-03	2.13E-07	−0.32	0.030	−0.16	0.054	0.01	0.062
01-06-01 Cañon Diablo										
GM3_CDT_1	4.50647E-02	5.77E-07	7.96E-03	3.01E-07	1.34	0.026	0.64	0.076	−0.06	0.080
GM3_CDT_2	4.50291E-02	4.76E-07	7.96E-03	2.72E-07	0.55	0.022	0.15	0.068	−0.13	0.072
GM3_CDT_3	4.50858E-02	3.41E-07	7.96E-03	2.03E-07	1.81	0.016	0.80	0.050	−0.14	0.054
GM3_CDT_4	4.50507E-02	5.22E-07	7.96E-03	1.95E-07	1.03	0.024	0.44	0.050	−0.10	0.054
GM3_CDT_5	4.50382E-02	6.54E-07	7.96E-03	1.85E-07	0.75	0.030	0.27	0.046	−0.12	0.054
04-21-01 Cañon Diablo										
GM3_CDT_1	4.50017E-02	6.39E-07	7.96E-03	1.62E-07	−0.06	0.028	−0.14	0.040	−0.10	0.050
GM3_CDT_2	4.49912E-02	5.50E-07	7.96E-03	1.56E-07	−0.30	0.024	−0.22	0.040	−0.06	0.046
GM3_CDT_3	4.50688E-02	6.35E-07	7.97E-03	2.73E-07	1.43	0.028	0.72	0.068	−0.02	0.074
GM3_CDT_4	4.50207E-02	6.24E-07	7.96E-03	1.85E-07	0.36	0.028	0.20	0.046	0.01	0.054
GM3_CDTb_1	4.49901E-02	8.48E-07	7.96E-03	1.78E-07	−0.32	0.038	−0.17	0.044	0.00	0.058
GM3_CDTb_2	4.49774E-02	7.21E-07	7.96E-03	2.13E-07	−0.60	0.032	−0.34	0.054	−0.03	0.062
GM3_CDTb_3	4.49816E-02	6.19E-07	7.96E-03	1.86E-07	−0.51	0.028	−0.25	0.046	0.01	0.054

Notes. Nomenclature is grain number + ion microprobe spot number. Error demagnification and corrections for instrumental mass bias were applied to the data (see text); Uncertainties in the ratios are reported at the 1σ level; the δ values (including $\Delta^{33}S$) are reported at the 2σ level ($n = 120$).

[a] $\delta^{34}S_{CDT} = 1000\ ((^{34}S/^{32}S)_{unknown}/(^{34}S/^{32}S)_{CDT} - 1)$. All values use the accepted reference ratio of Canon Diablo Troilite ($^{32}S/^{34}S$) = 22.220 (Ault and Jensen, 1962; cf. Ding et al., 2001).

[b] Errors derive from counting statistics and do not include the uncertainty in the composition of the standards in the small domains (<30 μm) analyzed by SIMS multicollection.

[c] Values for $(^{33}S/^{32}S)_{CDT}$ are determined separately for each analytical session (Table 4) by the intersection of the mass fractionation line on a three-isotope plot at $(\delta^{34}S_{CDT})/(\delta^{33}S) = 0$‰.

[d] $\Delta^{33}S = \delta^{33}S - 1000 \times (1 + \delta^{34}S/1000)^{0.515}$.

[e] Uncertainties were calculated using $[((2\sigma_{\delta 34S})^2 + (2\sigma_{\delta 33S})^2)^{1/2}] = (2\sigma_{\Delta 33S})$, which does not take into account error correlation (see text).

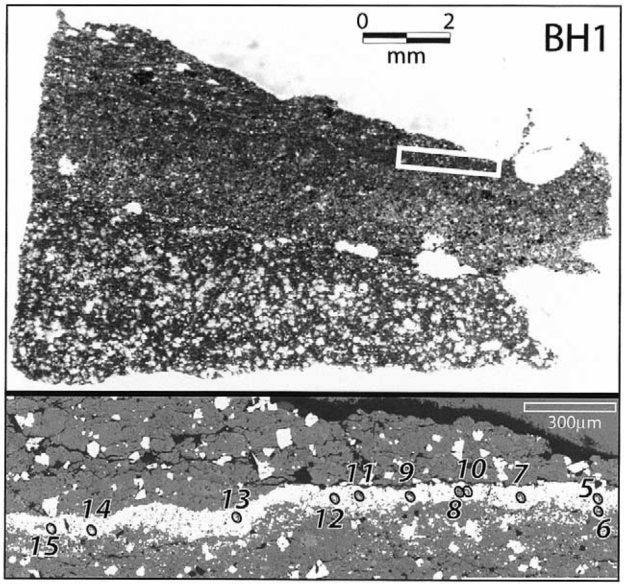

Fig. 3. (top) Optical micrograph of BIF sample *BH1*, Brockman iron formation, Hamersley Group, Western Australia (2.5 Ga). The sample is a finely layered chert/BIF with occasional bands of sulfides and phosphates interspersed in a matrix dominated by quartz, magnetite and hematite. The box in the thin section denotes the location of a pyrite microband in *BH1* (bottom) from which ion microprobe analyses of $\Delta^{33}S$ in situ were obtained (Table 5). Individual ion microprobe spots are labeled.

reveal $\Delta^{33}S$ in the sample is consistently negative (−1.7 to 0‰) with a >6‰ spread in $\delta^{34}S$ values (−6.1 to −0.8‰) preserved within an individual pyrite microband (Table 5; Fig. 3). A linear fit applied to the population of points with $\Delta^{33}S$ values that deviate from the mass fractionation line described by the standards, defines what we interpret as a separate mass-dependent fractionation array with slope $m = 0.52$ ($r^2 = 0.84$, s.d. = 0.51) and intercept at $\delta^{33}S = -0.84$‰ (Fig. 4).

3.2.2. *Cleaverville formation, Gorge Creek Group, Western Australia (PB6), ~3.2 to 3.3 Ga*

Red and black chert samples from the Gorge Creek Group at Point Samson, approximately 20 km northwest of Roebourne, Western Australia (Sugitani, 1992) were studied. Geochronology for the area has established an age of 3.3 Ga for the immediately underlying Wyman Fm. (Thrope et al., 1992) and an age of lower greenschist metamorphism of the Gorge Creek Group of 2.95 Ga (Oversby, 1976). Thus, the 3.2- and 3.3-Ga age of this formation is generally younger than rocks exposed in the eastern part of the Pilbara Block (Pidgeon, 1978). Sulfides are present as rare, small and isolated blebs of pyrrhotite; these were mapped by reflected light microscopy and characterized by EDS-EPMA before ion microprobe measurements (Fig. 5). Our analyses of chert sample *PB6* (sample 6 of Sugitani, 1992) reveal two points with large magnitude $\Delta^{33}S$ anomalies of opposite sign (−1.72 ± 0.34 and +1.31 ± 0.28‰, 2σ; Fig. 6). The scatter in the data might represent the

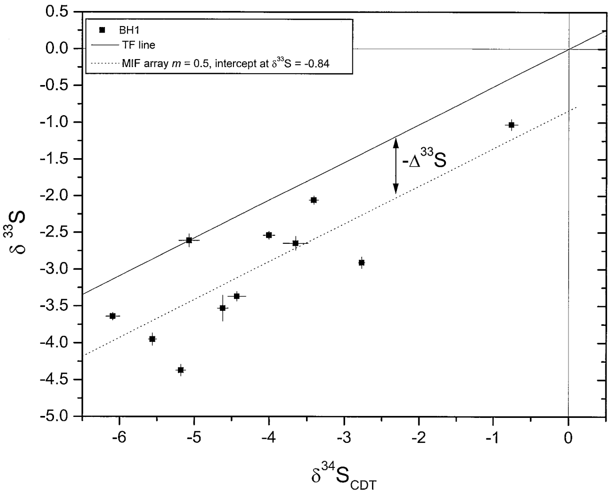

Fig. 4. δ^{33}S vs. δ^{34}S plot of *BH1* data. The majority of pyrites in this sample exhibit large negative Δ^{33}S anomalies ranging from -1.71 ± 0.08 to -0.01 ± 0.11‰ with a >6‰ spread in δ^{34}S values (-6.1 ± 0.1 to -0.8 ± 0.1‰) preserved within an individual pyrite microband (Fig. 3). A linear fit applied to the population of points with the greatest Δ^{33}S values defines a separate mass-dependent fractionation array of slope $m = 0.52$ ($r^2 = 0.84$, s.d. = 0.51, δ^{33}S-intercept at -0.84‰).

preservation in *PB6* pyrites of both sulfide and sulfate MIF reservoirs, but more data would be needed to support this hypothesis. The range of δ^{34}S seen was -0.3 to $+5.7$‰ (Table 5).

3.2.3. *Chert BIF, Isua Supracrustal Belt, West Greenland (GR97im23), ~3.8 Ga*

Chert and BIF form a large unit in the northeast limb of the arcuate 3.7 to 3.8 Ga Isua supracrustal belt (ISB) in West Greenland (Nutman et al., 1984, 1996, 1997b). Inferential geologic mapping carried out recently in the Isua region (Myers et al., 2001) has reiterated interpretations of protolith lithologies published over the last several years (Rose et al., 1996; Rosing et al., 1996) including a retrospective description of preserved pillow lava structures first reported in the early 1990s (Maruyama et al., 1991; Komiya et al., 1999). Rose et al. (1996) pointed out that much of the ISB has been altered by carbonation and potassic fluid metasomatism centered on mafic and ultramafic piles. Recently reported structural and paleodepositional studies (Fedo et al., 2001) build on previous

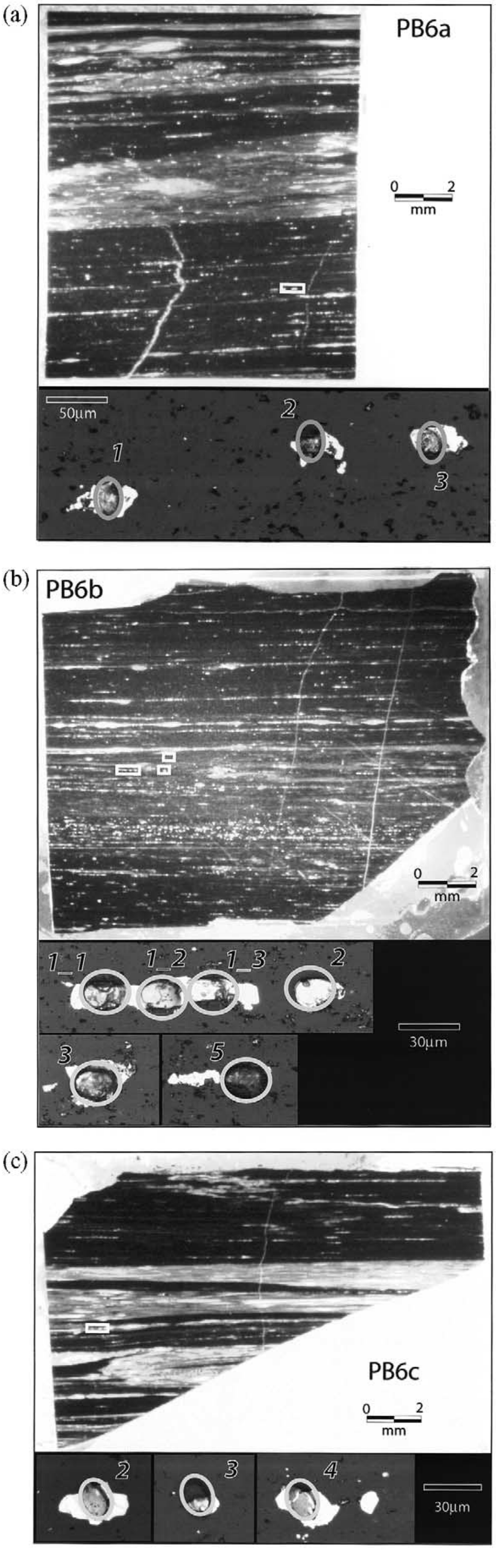

Fig. 5. (a) (top) Optical micrograph of banded chert sample *PB6a*, Cleaverville Formation, Gorge Creek Group, Western Australia (3.25 Ga). The sample is a finely layered black chert with rare individual (sulfide) pyrrhotite grains interspersed in a matrix dominated by quartz, kerogen, and minor magnetite. The box in the thin section denotes the location of three pyrrhotite grains (bottom) from which ion microprobe analyses of Δ^{33}S were obtained (Table 5). Individual ion microprobe spots are labeled in each figure (a–c). The range in δ^{34}S values in (a) was -0.3 ± 0.2 to $+4.7 \pm 0.3$‰. (b) Sample *PB6b*, similar to (a) with small (30 to 90 μm × 20 μm) pyrrhotites located parallel to bedding. The range in δ^{34}S values in (b) was $+0.5 \pm 0.3$ to $+3.4 \pm 0.1$‰. (c) Sample *PB6c*, the same in many respects to (a) and (b) except that in this sample, the pyrrhotites are very small (<50 μm), a testimony to the unique resolving power of the ion microprobe technique to measure Δ^{33}S at this scale of spatial resolution. The range in δ^{34}S values in (c) was $+4.0 \pm 0.1$ to $+5.7 \pm 0.4$‰.

Table 5. Sulfur isotopic compositions of Precambrian sulfides by in situ ion microprobe multicollection.

Grain_spot	$^{34}S/^{32}S$	±1σ	$^{33}S/^{32}S$	±1σ	$\delta^{34}S_{CDT}$[a] (‰)	±2σ (‰)	$\delta^{33}S_{CDT}$[b] (‰)	±2σ[c] (‰)	$\Delta^{33}S$[d] (‰)	±2σ[e] (‰)
05-24-00 BH1 banded iron-formation Hamersley Group, Dales Gorge Member, W. Australia 2.5 Ga pyrite (Figure 3)										
BH1_5_1	4.47544E-02	1.19E-06	7.92E-03	3.32E-07	−5.56	0.053	−3.95	0.084	−1.10	0.089
BH1_6	4.47713E-02	1.48E-06	7.92E-03	3.08E-07	−5.18	0.066	−4.37	0.078	−1.71	0.086
BH1_7	4.47305E-02	2.09E-06	7.93E-03	2.06E-07	−6.09	0.094	−3.64	0.052	−0.52	0.072
BH1_8	4.47966E-02	1.60E-06	7.93E-03	6.98E-07	−4.62	0.072	−3.53	0.176	−1.15	0.181
BH1_9	4.48799E-02	9.27E-07	7.93E-03	3.15E-07	−2.77	0.041	−2.91	0.079	−1.49	0.083
BH1_10	4.48509E-02	1.37E-06	7.94E-03	2.25E-07	−3.41	0.061	−2.06	0.057	−0.31	0.066
BH1_11	4.49703E-02	1.94E-06	7.95E-03	2.97E-07	−0.76	0.086	−1.03	0.075	−0.64	0.088
BH1_12	4.47762E-02	3.08E-06	7.94E-03	3.53E-07	−5.07	0.138	−2.61	0.089	−0.01	0.115
BH1_13	4.48244E-02	1.73E-06	7.94E-03	2.13E-07	−4.00	0.077	−2.54	0.054	−0.48	0.068
BH1_14	4.48049E-02	2.68E-06	7.93E-03	2.59E-07	−4.43	0.120	−3.37	0.065	−1.09	0.091
BH1_15	4.48403E-02	3.69E-06	7.93E-03	3.74E-07	−3.65	0.165	−2.65	0.094	−0.78	0.128
05-23-05-25-00 PB6 metachert. Pilbara Group, Roeburne Belt, W. Australia 3.2–3.3 Ga pyrrhotite (Figure 5)										
PB6a_1_1	4.49934E-02	3.56E-06	7.94E-03	1.33E-06	−0.25	0.158	−1.85	0.334	−1.72	0.346
PB6a_2_1	4.52167E-02	7.74E-06	7.98E-03	2.29E-06	4.71	0.343	2.81	0.575	0.39	0.603
PB6a_3_1	4.51220E-02	5.68E-07	7.96E-03	2.55E-07	2.6	10.025	0.90	0.064	−0.44	0.067
PB6b_1_1	4.51439E-02	2.59E-06	7.97E-03	6.34E-07	3.10	0.115	1.23	0.159	−0.36	0.172
PB6b_1_2	4.50971E-02	2.77E-06	7.97E-03	2.90E-07	2.06	0.123	1.57	0.073	0.52	0.098
PB6b_1_3	4.51012E-02	1.98E-06	7.97E-03	3.36E-07	2.15	0.088	1.25	0.084	0.15	0.098
PB6b_2_1	4.51562E-02	7.62E-07	7.97E-03	3.99E-07	3.37	0.034	1.71	0.100	−0.02	0.104
PB6b_3_1	4.51393E-02	1.03E-06	7.97E-03	3.63E-07	3.00	0.046	1.18	0.091	−0.36	0.096
PB6b_5_1	4.50253E-02	6.13E-06	7.97E-03	9.63E-07	0.46	0.272	1.55	0.242	1.31	0.281
PB6c_2	4.51867E-02	1.61E-06	7.97E-03	3.04E-07	4.05	0.071	2.18	0.076	0.10	0.087
PB6c_3	4.51990E-02	2.91E-06	7.98E-03	1.92E-07	4.32	0.129	3.02	0.048	0.80	0.084
PB6c_4	4.52593E-02	9.99E-06	7.98E-03	2.30E-06	5.66	0.441	2.66	0.576	−0.25	0.621
05-25-00 GR97IM23 banded iron-formation Isua Supracrustal Belt, W. Greenland −3.77 Ga pyrite (Figure 8)										
1_1	4.50227E-02	2.32E-06	7.97E-03	2.29E-07	0.40	0.103	1.95	0.058	1.74	0.079
1_2	4.50723E-02	2.84E-06	7.98E-03	3.09E-07	1.51	0.126	2.71	0.077	1.93	0.102
1_3	4.51046E-02	1.28E-06	7.98E-03	1.88E-07	2.22	0.057	2.97	0.047	1.83	0.056
1_4	4.50825E-02	2.96E-06	7.98E-03	3.22E-07	1.73	0.131	2.59	0.081	1.70	0.106
1_5	4.50783E-02	2.05E-06	7.98E-03	1.39E-07	1.64	0.091	2.76	0.035	1.92	0.059
1_6	4.50900E-02	1.42E-06	7.98E-03	2.82E-07	1.90	0.063	2.91	0.071	1.94	0.079
2_1	4.50943E-02	4.61E-07	7.98E-03	2.27E-07	2.00	0.020	2.97	0.057	1.95	0.059
2_2	4.50646E-02	2.09E-06	7.98E-03	2.91E-07	1.34	0.093	2.55	0.073	1.87	0.088
2_3	4.50563E-02	2.45E-06	7.97E-03	2.09E-07	1.15	0.109	2.35	0.052	1.76	0.077
2_4	4.50623E-02	1.33E-06	7.98E-03	3.03E-07	1.29	0.059	2.68	0.076	2.02	0.083
3_1	4.50839E-02	4.08E-06	7.98E-03	4.44E-07	1.76	0.181	2.64	0.111	1.74	0.146
4_1	4.50039E-02	5.15E-06	7.97E-03	4.38E-07	−0.01	0.229	1.33	0.110	1.34	0.162
5_1	4.50520E-02	1.01E-06	7.96E-03	5.17E-07	1.06	0.045	0.89	0.130	0.35	0.133
6_1	4.50782E-02	3.90E-07	7.96E-03	1.55E-07	1.64	0.017	0.70	0.039	−0.14	0.041
4_2	4.50719E-02	3.92E-06	7.97E-03	6.11E-07	1.50	0.174	2.39	0.153	1.62	0.178
5_2	4.50121E-02	1.81E-06	7.95E-03	3.19E-07	0.17	0.080	−0.17	0.080	−0.25	0.091
01-06-01 IM43 garnet-biotite schist (metapelite), Isua Supracrustal Belt, W. Greenland ~3.77 Ga pyrite (Figure 11)										
1_1	4.50250E-02	4.28E-07	7.97E-03	2.19E-07	0.46	0.019	1.46	0.055	1.22	0.059
1_2	4.49625E-02	5.85E-07	7.96E-03	2.20E-07	−0.93	0.026	0.70	0.055	1.18	0.062
1_3	4.50032E-02	1.08E-06	7.97E-03	3.23E-07	−0.03	0.048	1.15	0.081	1.16	0.095
1_4	4.50363E-02	5.32E-07	7.97E-03	2.02E-07	0.71	0.024	1.60	0.051	1.23	0.057
2_1	4.50116E-02	9.19E-07	7.97E-03	2.81E-07	0.16	0.041	1.18	0.071	1.10	0.083
2_2	4.50228E-02	5.10E-07	7.97E-03	2.96E-07	0.41	0.023	1.33	0.074	1.12	0.079
2_3	4.49864E-02	4.82E-07	7.96E-03	2.25E-07	−0.40	0.021	0.91	0.056	1.12	0.061
05-24-00 GR9707 banded iron-formation/metaquartzite Akilia, SW Greenland >3.83 Ga pyrrhotite and chalcopyrite (Figure 13)										
S1_1 (po)	4.49002E-02	4.91E-06	7.96E-03	3.45E-07	−2.32	0.219	0.28	0.087	1.47	0.144
S1_2 (po)	4.49471E-02	1.58E-06	7.95E-03	2.40E-07	−1.28	0.070	−0.16	0.060	0.49	0.072
S1_3 (po)	4.50037E-02	2.81E-06	7.96E-03	2.42E-07	−0.02	0.125	0.56	0.061	0.57	0.090
S1_4 (po)	4.50782E-02	1.06E-06	7.96E-03	3.05E-07	1.64	0.047	0.97	0.077	0.13	0.082
S1_5 (po)	4.49829E-02	1.00E-06	7.95E-03	2.84E-07	−0.48	0.045	−0.54	0.071	−0.30	0.077
S1_6 (ch)	4.47060E-02	3.56E-06	7.93E-03	2.38E-07	−6.63	0.159	−2.86	0.060	0.54	0.105
S1_7 (ch)	4.47037E-02	1.32E-06	7.93E-03	2.15E-07	−6.68	0.059	−3.70	0.054	−0.27	0.066
S1_8 (ch)	4.48365E-02	4.48E-07	7.94E-03	1.58E-07	−3.73	0.020	−1.84	0.040	0.08	0.045
S1_9 (ch)	4.49959E-02	1.66E-06	7.95E-03	3.66E-07	−0.19	0.074	−0.43	0.092	−0.33	0.103
S1_10 (ch)	4.49129E-02	3.43E-06	7.95E-03	3.19E-07	−2.04	0.153	−0.29	0.080	0.76	0.116
S2_1 (po)	4.52006E-02	1.82E-06	7.98E-03	2.68E-07	4.36	0.081	2.54	0.067	0.30	0.081
S2_2 (po)	4.52394E-02	1.18E-06	7.98E-03	1.49E-07	5.22	0.052	3.15	0.037	0.47	0.048
S2_3 (po)	4.51406E-02	4.74E-06	7.98E-03	2.72E-07	3.02	0.210	2.40	0.068	0.84	0.130

Table 5. (Continued)

Grain_spot	$^{34}S/^{32}S$	$\pm 1\sigma$	$^{33}S/^{32}S$	$\pm 1\sigma$	$\delta^{34}S_{CDT}$[a] (‰)	$\pm 2\sigma$ (‰)	$\delta^{33}S_{CDT}$[b] (‰)	$\pm 2\sigma$[c] (‰)	$\Delta^{33}S$[d] (‰)	$\pm 2\sigma$[e] (‰)
04-21-01 GR0063 Ameralik dyke, Akilia, SW Greenland ~2.7 Ga pyrite										
G1-s1	4.47874E-02	5.10E-07	7.94E-03	2.56E-07	−4.82	0.023	−2.49	0.064	0.01	0.069
G1-s2	4.47966E-02	3.90E-07	7.94E-03	2.45E-07	−4.62	0.017	−2.37	0.062	0.03	0.065
G1-s3	4.48063E-02	4.63E-07	7.94E-03	3.66E-07	−4.40	0.021	−2.26	0.092	0.03	0.096

Notes. Nomenclature is grain number + ion microprobe spot number. Error demagnification and corrections for instrumental mass bias were applied to the data (see text); S isotope ratios of the unknowns were calibrated against known standards; uncertainties in the ratios are reported at the 1σ level; the δ values (including $\Delta^{33}S$) are reported at the 2σ level.

[a] $\delta^{34}S_{CDT} = 1000\,((^{34}S/^{32}S)_{unknown}/(^{34}S/^{32}S)_{CDT} - 1)$. All values use the accepted reference ratio of Canon Diablo Troilite $(^{32}S/^{34}S) = 22.220$ (Ault and Jensen, 1962).

[b] Errors derive from counting statistics and do not include the uncertainty in the composition of the standards in the small domains (<30 μm) analyzed by SIMS multicollection.

[c] Values for $(^{33}S/^{32}S)_{CDT}$ are determined separately for each analytical session (Table 4) by the intersection of the experimentally determined mass fractionation line and the accepted $(^{32}S/^{34}S)_{CDT} = 22.22$ (Ault and Jensen, 1962).

[d] $\Delta^{33}S = \delta^{33}S - 1000 \times (1 + \delta^{34}S/1000)^{0.515}$.

[e] Uncertainties were calculated using $[((2\sigma_{\delta 34S})^2 + (2\sigma_{\delta 33S})^2)^{1/2}] = 1\,(2\sigma_{\Delta 33S})_{SIMS}$ and then incorporating the uncertainty in $\Delta^{33}S$ for each phase from the standards (Table 3) such that $2\sigma_{\Delta 33S} = ((2\sigma_{\delta 34S})_{SIMS}{}^2 + (2\sigma_{\delta 33S)STD}{}^2)^{1/2}$ (see text).

work (Bridgwater and McGregor, 1974; Allaart, 1976; Nutman et al., 1984; Nutman et al., 1996, 1997b; Rose et al., 1996; Rosing et al., 1996) that reduced the recognizable lithology of the ISB to ferruginous quartzite and oxide faces BIF and relatively minor quartzo-feldspathic and biotite schists dominated by a succession of amphibolitized pillow basalts extensively altered in places by silicification, carbonation and other metasomatic effects. The sample collected for this study is part of an approximately 5 × 10–m outcropping of a well preserved BIF in the central part of northeastern sector of the ISB and consists of millimeter- to centimeter-thick bands of coarsely crystallized quartz and magnetite (Fig. 7) that are somewhat deformed yet preserve the integrity of individual sedimentary bands.

Sulfides in *GR97im23* are present as small euhedral to subhedral clusters of pyrite (Fig. 8) surrounded by a mixed matrix of magnetite and quartz and parallel to the sense of banding in the rock. Along with BIF seen elsewhere and typical of Archean volcano-sedimentary successions, this rock is regarded as a chemical sediment that has been enriched in metals from volcanic sources (Dymek and Klein, 1988) and probably represents part of a relatively deep (>100 m) marine sedimentary facies derived from the oxidation of upwelled Fe(II)-rich seawater to ferro-ferri-oxyhydroxides (Braterman et al., 1983) and subsequent diagenetic transformation to magnetite. Enrichment of seawater in ferrous iron and the transformation to abundant Fe_3O_4 in marine sediments is considered a signature style of sedimentation under anoxic conditions on the early Earth when Fe(II) concentrations were high in seawater (Holland, 1984; Bjerrum and Canfield, 2002). Therefore, sulfides in this rock are interpreted to sample the sulfur cycling to the water column from atmospheric or magmatic exhalative sources at time of deposition in an early Archean (~3.8 Ga) ocean. Our repeat measurements reveal consistently large positive $\Delta^{33}S$ anoma-

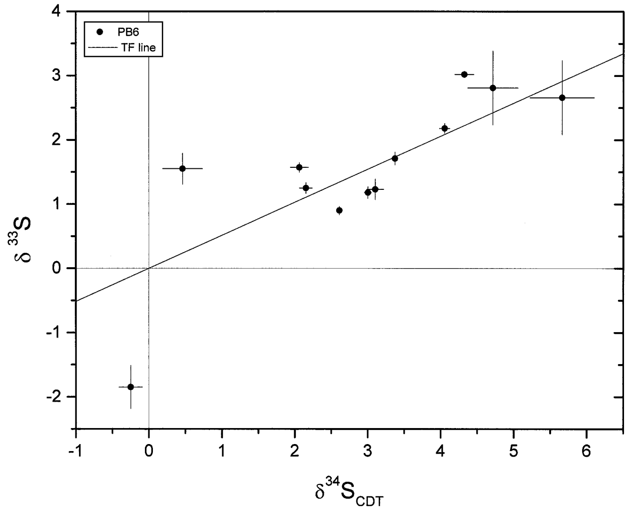

Fig. 6. $\delta^{33}S$ vs. $\delta^{34}S$ plot of *PB6* data. The majority of pyrrhotites in this sample plot close to the mass fractionation line with $\Delta^{33}S$ anomalies ranging from −0.36 ± 0.09 to +0.52 ± 0.10‰ with a ~6‰ spread in $\delta^{34}S$ values (−0.2 ± 0.2 to +5.7 ± 0.4‰) preserved overall (Table 5). No separate linear arrays are definable by these data.

Fig. 7. BIF sample *GR97im23* collected from the ~3.77-Ga ISB, West Greenland. Slightly deformed individual bands of magnetite are readily visible interposed between layers of quartz + grunerite.

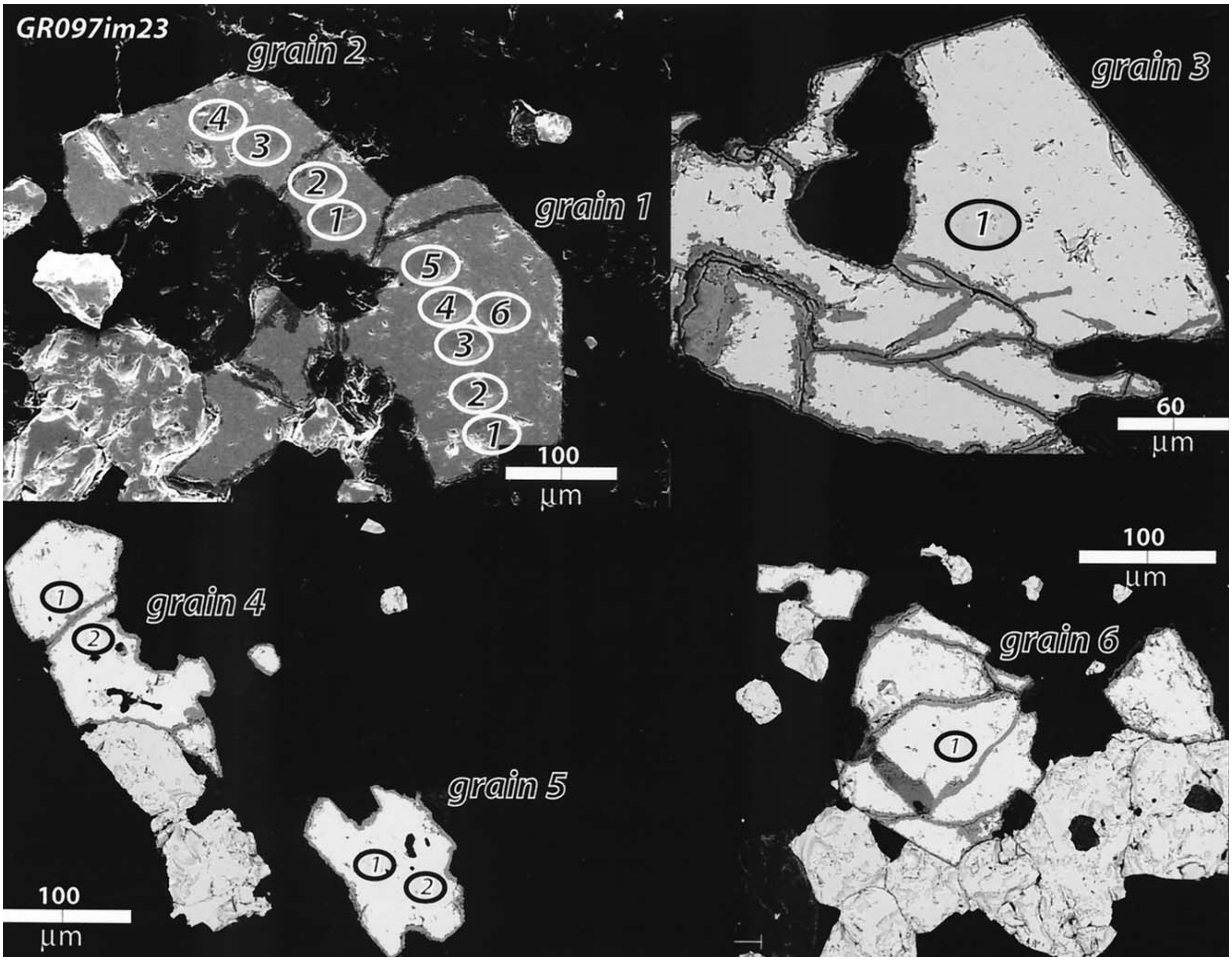

Fig. 8. Mixed secondary and backscattered electron images of pyrite grains 1 to 6 from BIF sample *GR97im23* from Isua. Scale bars are indicated. The petrology of the surrounding minerals is dominated by magnetite (to the left of sulfide grains 1 and 2, bottom of grain 4 and lower right of grain 6) and quartz. EPMA measurements on the low-contrast rims of the pyrite grains indicate they are composed of quartz, probably the result of silica mobility during metamorphism. Aside from sites 5_2 and 6_1 (Table 5), the pyrites in this sample had consistently positive Δ^{33}S anomalies. Ion microprobe traverses of grains 1 and 2 indicate that they may be subtly zoned in Δ^{33}S; further analyses are warranted to explore this possibility. Grains 5 and 6 had only small (but nonzero) anomalies in Δ^{33}S.

lies in *GR97im23* clustering mostly between $+2.02 \pm 0.082$ to $+1.34 \pm 0.161$‰ (2σ); these form a well defined linear array of slope $m = 0.694$ ($r^2 = 0.95$, s.d. $= 0.15$; Fig. 9). We note that the slope of this array is similar to the MIF slope derived from SO_2 photooxidation experiments by Farqhuar et al. (2000) describing the relationship $(1 + \delta^{33}S/1000) = (1 + \delta^{34}S/1000)^{0.649 \pm 0.006}$ and would therefore be consistent with photochemical models for the formation of BIF in an open ocean away from detrital sediment sources on the early Earth. Only a small, 2‰, range of δ^{34}S was observed in *GR97im23* pyrite (Table 5).

3.2.4. *Garnet–Biotite Schist, ISB, West Greenland (GR97im43), ~3.8 Ga*

Units originally described as Fe-Mg-rich quartz + plagioclase + biotite + garnet ± muscovite ± allanite schists and composing part of the original sequence B mica schist unit of Nutman et al. (1984) were collected in an effort to obtain rocks of pelitic origin from the ISB. A large (~5-kg) sample was collected from an upper unit in the sequence (Fig. 10), which contains layer of predominantly of garnet–biotite schist (≈ ferruginous metapelite; Dymek and Klein, 1988). The protolith of this rock was most likely a fine-grained siltstone deposited in a deep marine setting, perhaps derived from submarine or subaerial weathering of mafic volcanic piles. Sulfides are rare but recognizable in the hand sample and are present as small, isolated anhedral blebs of pyrite (Fig. 11) parallel to schistosity. We hypothesize that in the absence of a widespread detrital mineral component and with the fine-grained texture of the rock and a mineral composition consistent with a pelitic origin, sulfides in this rock displaying resolvable Δ^{33}S anomalies could represent some fraction of the mass-independently fractionated sulfur aerosol flux to the open ocean at time of deposition of the sediment at ~3.8 Ga.

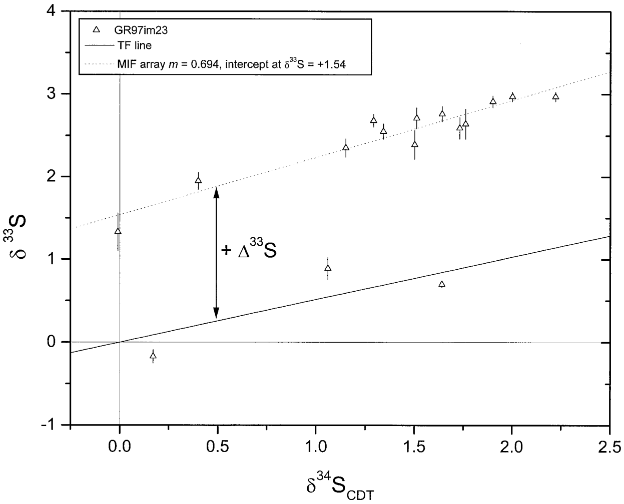

Fig. 9. δ^{33}S vs. δ^{34}S plot of *GR97im23* data. All pyrites in this sample, with the exception of 5_1, 5_2, and 6_1, exhibit large positive Δ^{33}S anomalies ranging from +1.34 ± 0.16 to +2.02 ± 0.08‰ with a small ~ 2‰ spread in δ^{34}S values (+2.2 ± 0.1 to 0.0 ± 0.3‰, Table 5). A linear fit applied to the population of points with the greatest Δ^{33}S values defines a separate linear array of slope $m = 0.694$ ($r^2 = 0.95$, s.d. = 0.15, δ^{33}S-intercept at +1.54‰). The slope of this array is similar to the MIF slope derived from SO_2 photooxidation experiments that describe the relationship $(1 + \delta^{33}S/1000) = (1 + \delta^{34}S/1000)^{0.649 \pm 0.006}$ (Farquhar et al., 2000, 2001a).

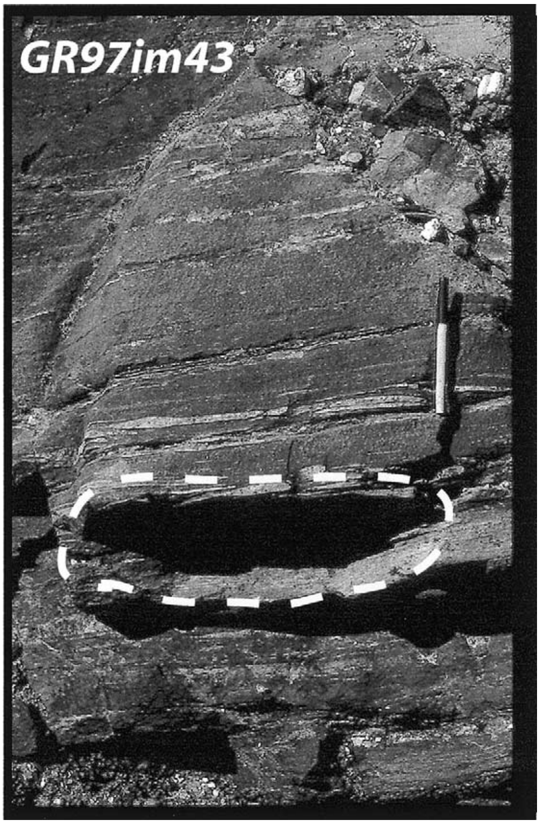

Fig. 10. Field photograph showing the exact sampling location (outline in shadow) of ferruginous metapelite *GR97im43* collected in the upper part of the B2 mica schist unit (Nutman et al., 1984) from the ~3.8-Ga ISB, West Greenland. Pen (for scale) is approximately 13.5 cm long.

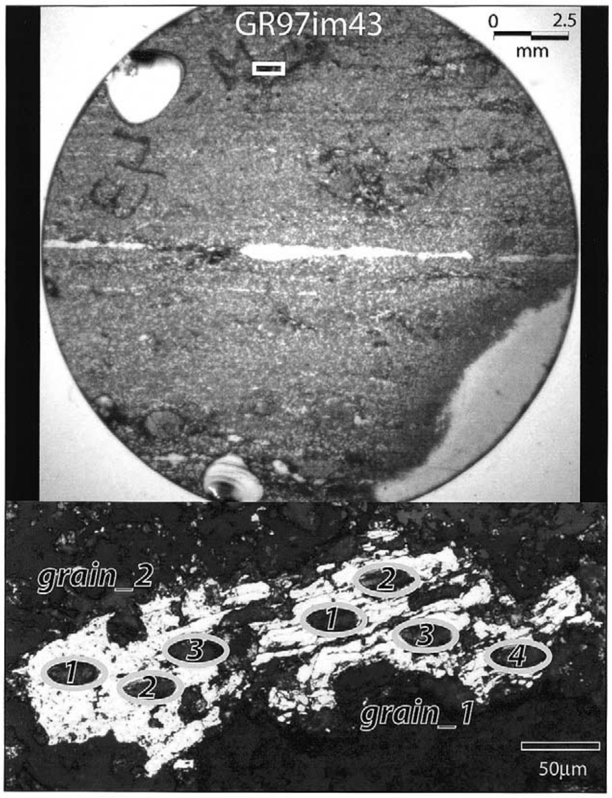

Fig. 11. (top) Round probe thin section of *GR97im43*; horizontal banding indicates sense of schistosity. The mineralogy is quartz + plagioclase + biotite + garnet ± muscovite ± allanite ± pyrite with minor graphite, magnetite, pyrite, and zircon(?). The box in the thin section denotes the location of two connected pyrite grains (bottom) from which ion microprobe analyses of Δ^{33}S in situ were obtained (Table 5). Individual ion microprobe spots are labeled in each grain. The total range in δ^{34}S values was −0.9 ± 0.1 to +0.7 ± 0.1‰. The pyrites in *GR97im43*had consistently positive Δ^{33}S anomalies. Ion microprobe traverses of grains 1 and 2 do not indicate zonation in Δ^{33}S.

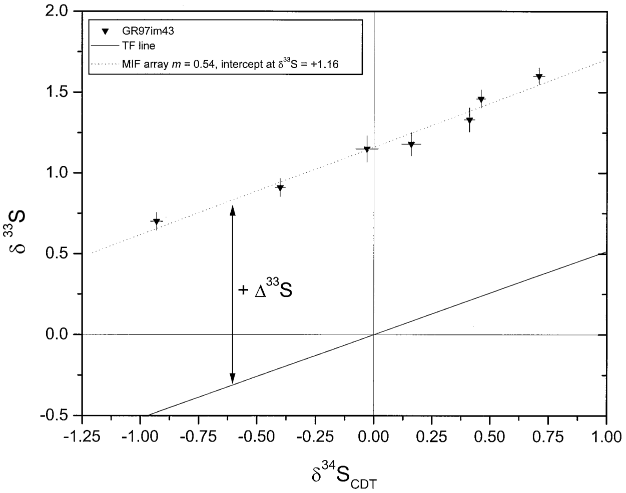

Fig. 12. δ^{33}S vs. δ^{34}S plot of *GR97im43* data. All pyrites from this sample exhibit large and consistently positive Δ^{33}S anomalies clustering between +1.23 ± 0.06 to +1.10 ± 0.08‰ (2σ) that form a linear array of slope $m = 0.54$ ($r^2 = 0.98$, s.d. = 0.056; δ^{33}S-intercept at +1.16‰) that resembles that predicted for mass-dependent fractionation (Bigeleisen and Mayer, 1947; Hulston and Thode, 1965).

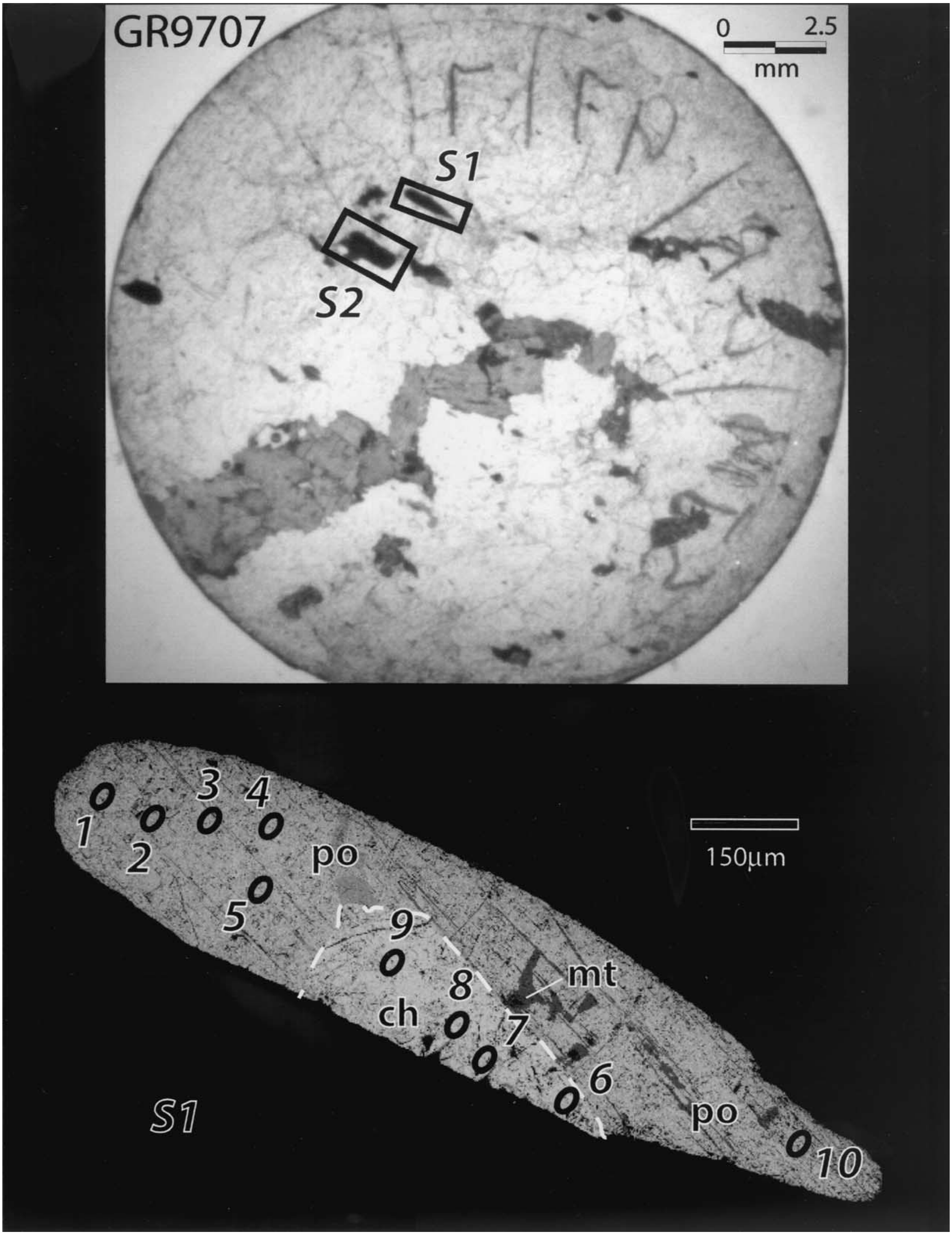

Fig. 13. (a) (top) Round probe thin section of Akilia quartz–magnetite metasediment *GR9707*. The mineralogy is quartz + magnetite + amphibole ± orthopyroxene ± garnet with minor apatite and graphite. The boxes in the thin section denote the location of two large sulfide (pyrrhotite + chalcopyrite) grains (S1 and S2) from which ion microprobe analyses of Δ^{33}S were obtained (Table 5). (bottom) Mixed secondary and backscattered electron images of pyrrhotite grain S1 from Akilia showing a traverse of grain S1 with individual ion microprobe spots labeled. The total range in δ^{34}S values for S1 was -2.3 ± 0.2 to $+1.6 \pm 0.1$‰ in pyrrhotite (po) and -6.6 ± 0.2 to -0.2 ± 0.1‰ in chalcopyrite (ch). One pyrrhotite spot in *GR9707* S1 had a large positive Δ^{33}S anomaly (+1.47‰) that may indicate that this grain is zoned in Δ^{33}S. (b) Mixed secondary and backscattered electron images of large (900 × 340 μm) pyrrhotite grain S2 from Akilia. The total range in pyrrhotite (po) δ^{34}S values for S2 was $+3.0 \pm 0.2$ to $+5.2 \pm 0.1$‰; chalcopyrite (ch) was not analyzed. mt = magnetite.

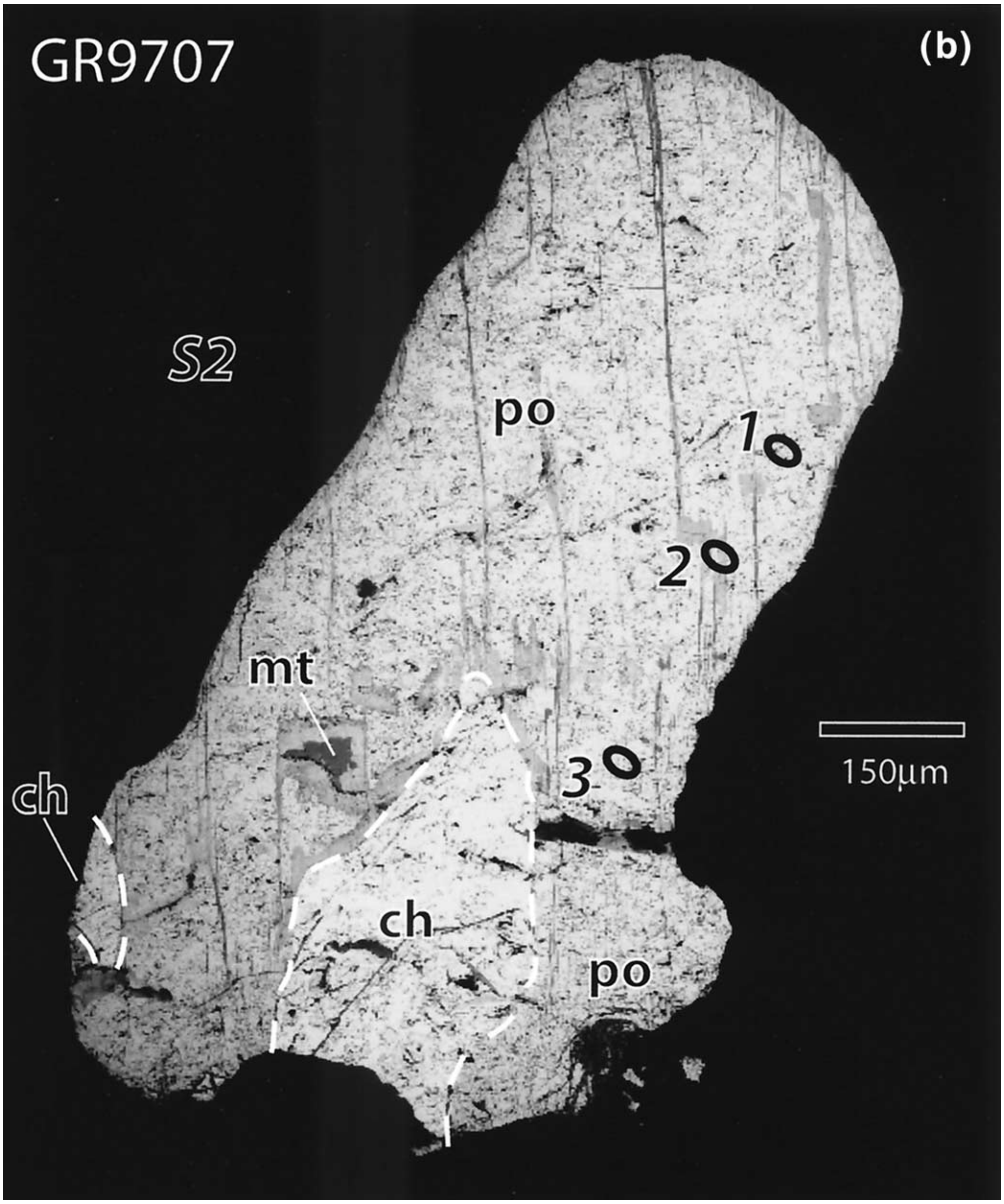

Fig. 13. (Continued)

Measurements of pyrites in *GR97im43* reveal large and consistently positive $\Delta^{33}S$ anomalies clustering between +1.23 to +1.10‰ that, grouped together, form a well-defined linear array of slope $m = 0.54$ ($r^2 = 0.98$, s.d. = 0.056; Fig. 12) similar to that expected for mass-dependent fractionation (Bigeleisen and Mayer, 1947; Hulston and Thode, 1965). The small range of $\delta^{34}S$ observed in *GR97im43* pyrite was −0.9 to +0.7‰ (Table 5).

3.2.5. *Fe-Rich Quartzite, Akilia (Island), Southern West Greenland (GR9707), ≥3.83 Ga*

A unit of layered amphibolite, ultramafic rocks of komatiitic composition (McGregor and Mason, 1977; Anbar et al., 2001) and quartz-magnetite metasediment occurs as a large tabular enclave in orthogneisses on the southwestern corner of Akilia (island) in southern West Greenland (McGregor and Mason, 1977). These rocks experienced granulite facies metamorphism (P > 5 kbar, T ~800°C) in the early Archean (Griffin et al., 1980; Nutman et al., 1997a) but underwent retrograde amphibolite-facies metamorphism in the late Archean, ~2700 Ma (Nutman et al., 1996). The magnetite-bearing quartzite on Akilia, which is overprinted by several generations of pyroxenite veinings (McGregor and Mason, 1977; Nutman et al., 1996, 1997a; Mojzsis and Harrison, 2002b; cf. Fedo and Whitehouse, 2002a,b) from the surrounding ultramafic units as well as intercalated Fe-rich pyroxenes typical of metamorphosed quartz-magnetite rocks (McGregor and Mason, 1977; Nutman et al., 1997a; Palin, 2002; Friend et al., 2002), is interpreted to be a highly deformed Fe-poor BIF (Nutman et al., 1997a).

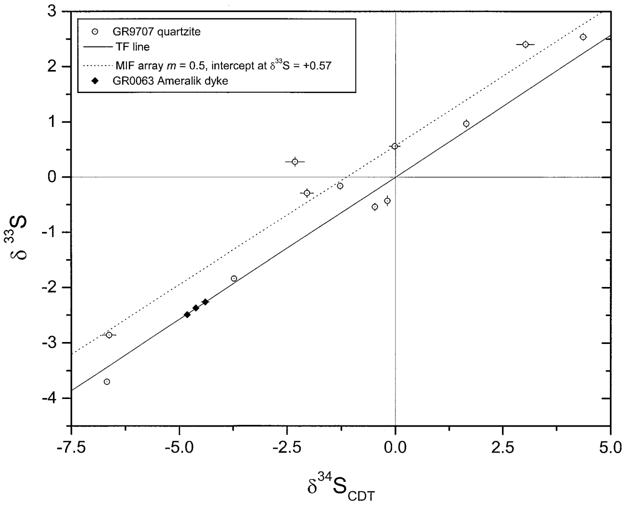

Fig. 14. δ^{33}S vs. δ^{34}S plot of *GR9707* data. Most *GR9707* sulfides exhibit positive Δ^{33}S anomalies clustering between +0.84 ± 0.13 to +0.30 ± 0.08‰ (2σ) and form a linear array of slope $m = 0.50$ ($r^2 = 0.99$, s.d. = 0.196; δ^{33}S-intercept at +0.57‰), the same as that predicted for mass-dependent fractionation (Bigeleisen and Mayer, 1947; Hulston and Thode, 1965). Three other points are somewhat negative (−0.33 ± 0.10, −0.30 ± 0.08, −0.27 ± 0.06‰ [2σ]). The relatively large range of δ^{34}S observed in the pyrrhotite and chalcopyrite for this rock was −6.7 ± 0.1 to +5.2 ± 0.1‰. Pyrites analyzed in the Ameralik dyke (*GR0063*) are also shown (Table 5) and contain no Δ^{33}S anomalies to the limits of our resolution. This result is consistent with an igneous intrusive origin of the Ameralik dykes and a magmatic value of Δ^{33}S = 0‰.

Sulfides in *GR9707* occur as rare, isolated anhedral blebs of pyrrhotite + chalcopyrite (Fig. 13) associated with magnetite.

Measurements of both pyrrhotite (po) and chalcopyrite (ch) in the >3.83 Ga (Mojzsis and Harrison, 2002a) sample *GR9707* reveal a large positive Δ^{33}S anomaly at +1.47 ± 0.14‰ (2σ). A population of positive Δ^{33}S values ranging between +0.84 to +0.30‰ can be grouped together to form a linear array of slope $m = 0.50$ ($r^2 = 0.99$, s.d. = 0.196; Fig. 14) similar to that predicted for mass-dependent fractionation. Three other points have slightly negative Δ^{33}S values (−0.33 ± 0.099, −0.30 ± 0.075, −0.27 ± 0.062‰ [2σ]), but we cannot confidently assign a mass-dependent ($m \approx 0.5$) relationship to them because they are so close to the mass fractionation line. A relatively large range (~12‰) of δ^{34}S was observed in *GR9707* pyrrhotite and chalcopyrite: −6.7 to +5.2‰ (Table 5).

As a means of testing whether high-grade metamorphism or metasomatism with S-bearing fluids might have played a role in modifying Δ^{33}S among different lithological units on Akilia, we sampled one of the many Archean (>3.1 Ga) Ameralik dykes that structurally cross-cut the early Archean lithologies, including the supracrustal package containing quartz-magnetite sample *GR9707*. As seen in Table 5 and Figure 14, pyrites analyzed in the Ameralik dyke (*G1*) contain no Δ^{33}S anomalies to the limits of our resolution, consistent with their igneous intrusive origin and a magmatic value of Δ^{33}S = 0‰. The results from the Ameralik dyke sample *G1* are in marked contrast with those obtained on the metaquartzite sample *GR9707* and provides further evidence for the sedimentary origin of the quartzite from Akilia.

4. DISCUSSION

Multicollector ion microprobe measurements of δ^{33}S and δ^{34}S and the observed MIF composition in sulfides corroborate previously reported Δ^{33}S anomalies in sulfide and sulfate from ancient sedimentary rocks (Farquhar et al., 2000). Figure 15 plots our new ion microprobe Δ^{33}S data with previously reported results from a host of sedimentary and metasedimentary rocks and significantly adds to the data set for multiple sulfur isotopes for pre-3.5 Ga rocks. It is apparent from Figure 15 that the data track a major change in sulfur geochemistry sometime between 1.9 to 2.4 Ga related to the demise of the Δ^{33}S signal in sediments. The δ^{33}S/δ^{34}S composition of samples measured by Farquhar et al. (2000) and in this study by ion microprobe that are older than ~2.4 Ga display MIF signatures with a total range of values between Δ^{33}S = −1.72 ± 0.34‰ (2σ) and +2.02 ± 0.08‰ (2σ). Younger samples, represented by our standards data set as well as sulfides in igneous rocks (e.g., *GR0063*) fall within a relatively small range about Δ^{33}S ≈ 0‰. The origin of the MIF effect in sulfur on early Earth and Mars, as revealed by measured Δ^{33}S anomalies, is postulated to be from gas phase reactions in planetary atmospheres. Experimental (Farquhar et al., 2001a) and model (Pavlov and Kasting, 2002) studies that seek to identify the conditions necessary to produce MIF δ^{33}S/δ^{34}S, which are transferred to surface materials (e.g., surface minerals, sediments, waters, and ices), hold the potential for exploring past atmospheric chemical evolution in the preserved rock record. The full implications of these results remain to be realized as our understanding of the specific reaction pathways for mass-independent isotope fractionation improves (Thiemens et al., 2001).

4.1. Ancient Terrestrial Atmospheric Oxygen

Quantitative constraints on the oxygen concentration of the Archean atmosphere based on atmospheric model calculations coupled with investigations of the geologic record have been sought after for many years. The chemical nature of the Archean atmosphere is critical to the understanding of Archean geology and of atmospheric evolution in general. The current paradigm states that the free oxygen levels of early atmospheres were much lower ($pO_2 \ll 10^{-2}$ present atmospheric level, PAL) before ~2.3 Ga (Cloud, 1972; Walker, 1977; Walker et al., 1983; Holland, 1984, 1994, 1999; Kasting, 1992, 1993, 2001; Rye et al., 1997; Rye and Holland, 1998; Farquhar et al., 2000; Pavlov and Kasting, 2002). An alternative view argues that the atmosphere was oxygen rich, or at least away from anoxic, throughout the Archean (Dimroth and Kimberley, 1976; Towe, 1990; Ohmoto, 1996, 2001; Watanabe et al., 1997). A major review of the geological record of atmospheric evolution noted several pieces of evidence as important for establishing the case for an anoxic atmosphere before approximately 2.3 Ga (Holland, 1984) highlighting in particular the study of detrital gold, uraninite, and pyrite grains in pre-2.3 Ga sediments (cf. Barnicoat et al., 1997). Geochemical indicators (Fe^{2+} vs. Fe^{3+}) in paleosols (Holland, 1994; Rye and Holland, 1998; Rasmussen and Buick, 1999), arguments regarding the origin and possible mode of deposition of BIF (Cloud, 1972), and of carbon isotope signatures in Precambrian organic matter (DesMarais, 1997) and carbonates (Karhu and Holland, 1996)

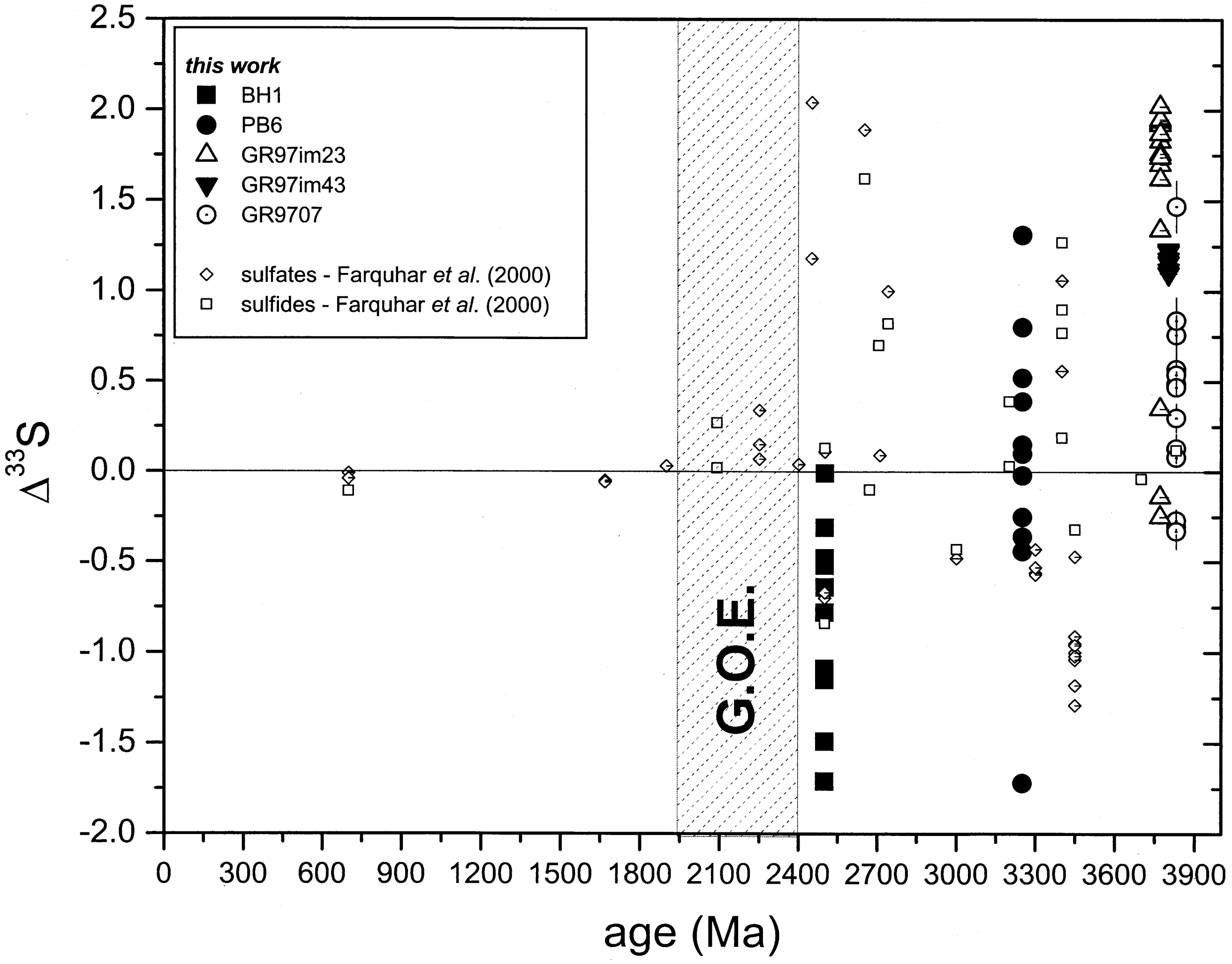

Fig. 15. Sulfur multiple isotope data (expressed as $\Delta^{33}S$) for sedimentary sulfides and sulfates as a function of age (replotted from Farquhar et al., 2000). Added to these values are the new data reported in this work (from Table 4). A large range in $\Delta^{33}S$ values in samples >2.4 Ga in age most likely reflects a change in atmospheric chemistry in the 1.9- to 2.4-Ga interval (stippled box) as a result of the marked oxidation of the surface zone of the Proterozoic Earth over the course of the Great Oxygenation Event (GOE).

have also been used to support models for an early anoxic atmosphere on Earth (cf. Ohmoto, 1999).

The MIF behavior of sulfur in gas phase reactions in anoxic atmospheres can potentially provide three independent constraints on the oxygen content of early atmospheres.

(1) Separate mass-dependent arrays ($m \approx 0.5$) within MIF $\delta^{33}S/\delta^{34}S$ data derived from ancient sulfides presented here argue against effective pyrite oxidation and homogenization of both reduced sulfur and (oxidized) sulfate reservoirs by biologic cycling or inorganic processes. The first-order result of this constraint essentially supports the conclusions based on paleosol and detrital mineral data that $pO_2 \leq 10^{-4}$ PAL before ~2.3 Ga and that sulfate was of relatively limited availability in the oceans for sulfate reduction by bacteria.

(2) Experiments to delimit the range of conditions necessary for 190- to 220-nm ultraviolet photolysis of SO_2 in the lower atmosphere and the lifetime of this reaction under various parameters have succeeded in producing large MIF signatures that mimic those observed in ancient sulfides (Farquhar et al., 2001a). These results suggest that whole-atmosphere column abundances of O_3 and O_2 were so low that 190- to 220-nm radiation could penetrate deep into the pre-2.3-Ga atmosphere. Consequently, the mere presence of anomalous $\Delta^{33}S$ can be used to place qualitative upper limits of oxygen concentrations of approximately 10^{-1} to 10^{-2} PAL.

(3) Because the only fractionation mechanism that appears to be consistent with the multiple isotope data for sulfur involves atmospheric reactions such as SO_2 photolysis, chemical models must be developed that provide mechanisms for the transfer of MIF signatures to the surface in early anoxic atmospheres. Recent theoretical work (Pavlov and Kasting, 2002) demonstrates that the MIF signatures of sulfur aerosols are preserved from homogenization in oceanic sulfate reservoirs only in atmospheres with $pO_2 < 10^{-5}$. An important conclusion from these model studies is that it is not possible to create anomalous $\delta^{33}S/\delta^{34}S$ in a high pO_2 atmosphere; the cessation of MIF signatures on sedimentary sulfur appears essentially complete in these models even before the $pO_2 = 10^{-5}$ PAL threshold is reached.

In both the experimental (2) and theoretical (3) models cited above, it is presumed that the magnitude of the $\Delta^{33}S$ anomaly

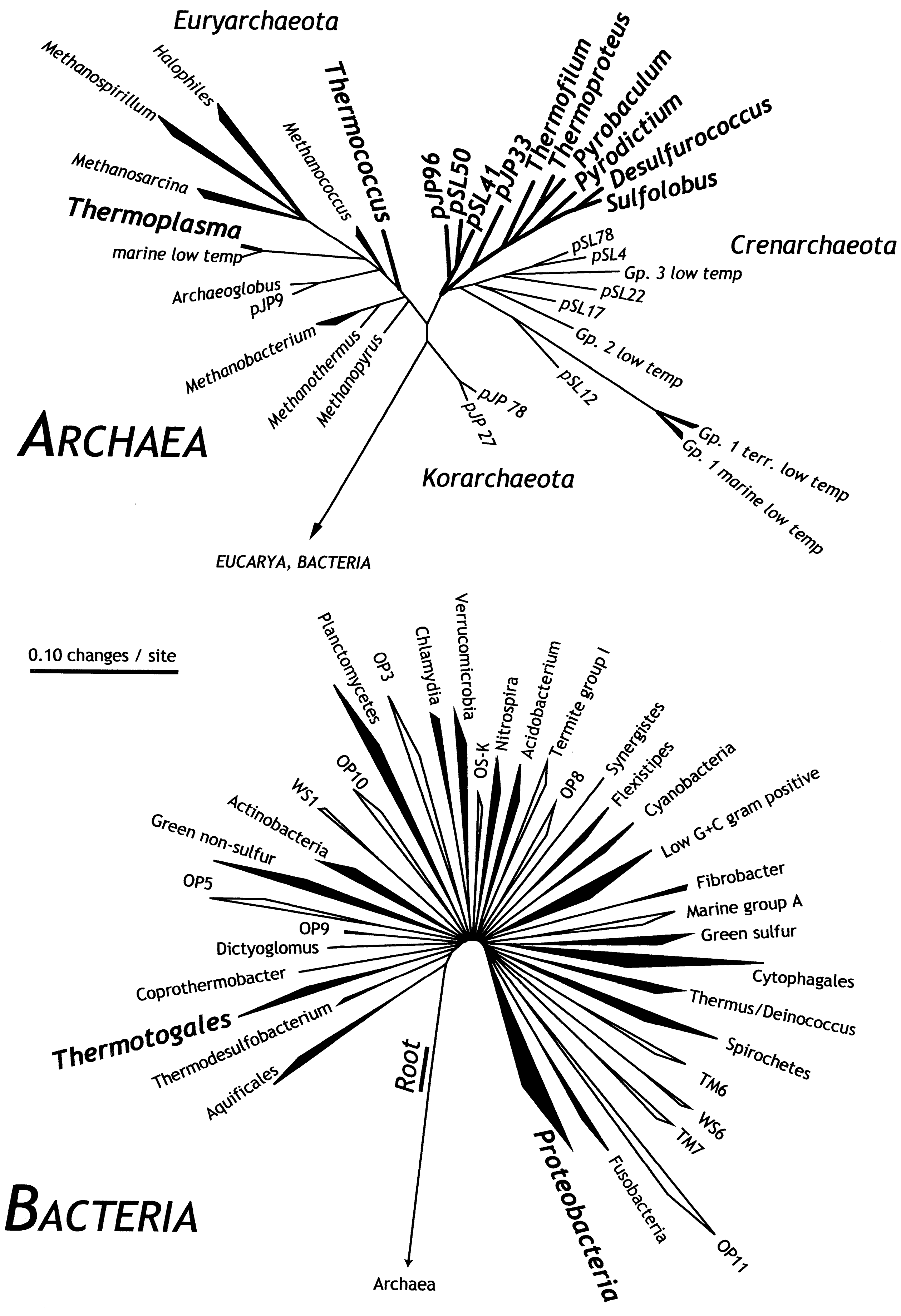
Euryarchaeota
Methanospirillum
Halophiles
Methanosarcina
Thermoplasma
marine low temp
Archaeoglobus
pJP9
Methanobacterium
Methanothermus
Methanopyrus
Methanococcus
Thermococcus
pJP96
pSL50
pSL41
pJP33
Thermofilum
Thermoproteus
Pyrobaculum
Pyrodictium
Desulfurococcus
Sulfolobus
Crenarchaeota
pSL78
pSL4
Gp. 3 low temp
pSL22
pSL17
Gp. 2 low temp
pSL12
Gp. 1 terr. low temp
Gp. 1 marine low temp
pJP 78
pJP 27
Korarchaeota
ARCHAEA
EUCARYA, BACTERIA
0.10 changes / site
Planctomycetes
OP3
Chlamydia
Verrucomicrobia
OS-K
Nitrospira
Acidobacterium
Termite group I
OP8
Synergistes
Flexistipes
Cyanobacteria
Low G+C gram positive
Fibrobacter
Marine group A
Green sulfur
Cytophagales
Thermus/Deinococcus
Spirochetes
TM6
WS6
TM7
OP11
Fusobacteria
Proteobacteria
Root
Archaea
Aquificales
Thermodesulfobacterium
Thermotogales
Coprothermobacter
Dictyoglomus
OP9
OP5
Green non-sulfur
Actinobacteria
WS1
OP10
BACTERIA

Fig. 16. Phylogenetic trees of Archaea and Bacteria based on small-subunit (SSU) ribosomal RNA sequences (from Pace, 2001). The scale bar represents approximately 0.1 changes per nucleotide. (top) Diagrammatic representation of the phylogeny of Archaea. Wedges indicate that several representative sequence groups of organisms fall within the indicated depth of branching. Names correspond to organisms or groups of organisms. (bottom) Diagrammatic representation of the phylogenetic divisions of the diverse Bacteria; open wedges are environmental sequences named after clone libraries; solid wedges represent cultured organisms. In these figures, organisms that are known to reduce elemental sulfur (S^0, S^8) to H_sS are labeled in boldface type; their branches are likewise boldface. The deep-branching of this metabolic style in both Bacteria and Archaea points to an ancient origin (Stetter and Gaag, 1983), probably at the last common ancestor (labeled "root," in Bacteria) of all life. The organisms that reduce elemental sulfur are hyperthermophilic, suggesting that this metabolism may have evolved in a high-temperature environment (Stetter, 1996).

is directly proportional of the residence time of reactive sulfur species (e.g., SO_2) in the atmosphere, balanced with the surface deposition of its reaction products including elemental sulfur (Pavlov and Kasting, 2002). However, much work needs to be done before this aspect can be quantified. Thus, finding diverse $\Delta^{33}S$ anomalies in a varied suite of Archean and early Proterozoic marine sedimentary sulfides would stipulate that the sulfur measured was cycled through an atmosphere with very low oxygen concentration and that this was a major source of sulfur to seawater on the early Earth. Our data (Fig. 15) are therefore consistent with an anoxic ($<10^{-5}$ PAL), photochemically active atmosphere before the mid to early Proterozoic and extending to the oldest sediments.

4.2. Implications for Early Life Environments

Comparative sequence analyses of genomes are used to infer phylogenetic relationships between organisms (Woese, 1987, 2000) and their evolutionary history in terms of molecular biology (Pace, 1997, 2001). Such analyses define three Domains within the rRNA Phylogenetic Tree of Life: Bacteria, Archaea, and Eucarya. Many hyperthermophilic, deep-branching organisms in Bacteria (Thermotogales) and in Archaea (sub-Domain Crenarcheota; *Pyrococcus* and *Thermoplasma* in sub-Domain Euryarcheota) reduce elemental sulfur (S^0) to H_2S using both H_2 and organic compounds as an electron donor. The antiquity of this metabolic pathway is evident in that both deep-branching Bacterial and Archaeal lineages share this feature (Stetter and Gaag, 1983; Stetter, 1996; Canfield and Raiswell, 1999; Fig. 16). Thus, these observations suggest that elemental sulfur reduction is an inherited trait from the last common ancestor of all life. Currently, these organisms obtain elemental sulfur from rapid cooling of volcanogenic sulfurous gases where $2SO_2 + 2H_2S^0 \leftrightarrow 4S^0 + 2H_2O$; this shifts the equilibrium in favor of S^0 (Grinenko and Thode, 1970), which is metabolically available for reduction to H_2S.

As pointed out in Farquhar et al. (2001a), a consequence of the model for anomalous $\Delta^{33}S$ sulfur aerosol formation is that pyrite forming via sulfur reduction by organisms to H_2S would retain positive $\Delta^{33}S$ signatures, whereas pyrite formed from sulfate reduction would be expected to preserve negative $\Delta^{33}S$ values. The latter case may be seen in our data for *BH1* a ~2.5 Ga BIF where the pyrites are consistently negative (Fig. 4) and a linear fit applied to data defines a separate mass-dependent fractionation array that may be consistent with an origin by microbial sulfate reduction, although the total range in $\delta^{34}S$ ($\leq$6‰) is smaller than that typically assigned to biologic fractionation (Canfield and Raiswell, 1989). It is worth noting that in our most ancient samples (including *GR9707*), the majority of pyrites have strongly positive $\Delta^{33}S$ values, which we interpret to be inconsistent with sulfate reduction and if biologically mediated (with a spread in $\delta^{34}S$ values greater than ~10‰), would be more in line with elemental sulfur reduction.

The mere presence in our data of strongly positive $\Delta^{33}S$ anomalies with separate linear arrays provides a compelling case that the source of sulfur in these systems was cycled through the atmosphere and introduced to the oceans in the early Archean and isolated there from rehomogenization by volcanic and hydrothermal sources of sulfur. Elemental sulfur (S^0, S^8) aerosols (Pavlov and Kasting, 2002) derived from atmospheric reactions and deposited into the oceans would have provided a ready source of sulfur to a plethora of microbial environments at the global scale (Fig. 17). Significantly, the oldest sample we studied, *GR9707* a ≥3.83-Ga quartz + magnetite rock from Akilia, has a separate mass-dependent fractionation array similar to the ferruginous metapelite *GR97im43* from the ISB, but with a range in $\delta^{34}S$ of ~12‰. We interpret this range to most likely be a reflection of hydrothermal fractionation of the isotopes during multiple metamorphic events, although elemental sulfur reduction by metabolic processes at time of deposition cannot be ruled out.

Sample *GR97im23*, a BIF from Isua has a small (2‰) range in $\delta^{34}S$, but in three-isotope space, it defines a separate linear array with a slope inconsistent with mass-fractionation. We propose that these sulfides result from the extremely rapid deposition of sulfur aerosols into the early Archean ocean followed by sedimentation as pyrite under anoxic and reducing conditions. A case for biologic sulfur reduction in the samples analyzed cannot be made at this time on the basis of the limited data set. More measurements are needed of early Archean sediments and of putative sulfidic microfossil forms (Rasmussen, 2000) in the search for definite evidence for this ancient metabolic style.

4.3. Sedimentary Origin of Akilia Quartz + Magnetite Lithologies

4.3.1. *Geochronological constraints*

Because of the importance of the Akilia rock in terms of evidence for early biologic activity (Mojzsis et al., 1996) and a recent debate concerning the minimum age of its deposition, it is relevant to provide background geochronological information for this sample. Supracrustal rocks such as the Akilia quartzite that have undergone high-grade metamorphism are not used for precise and accurate whole-rock geochronology because of open-system behavior of Rb-Sr, Sm-Nd, and U-Pb during metamorphism. It is therefore necessary to resort to

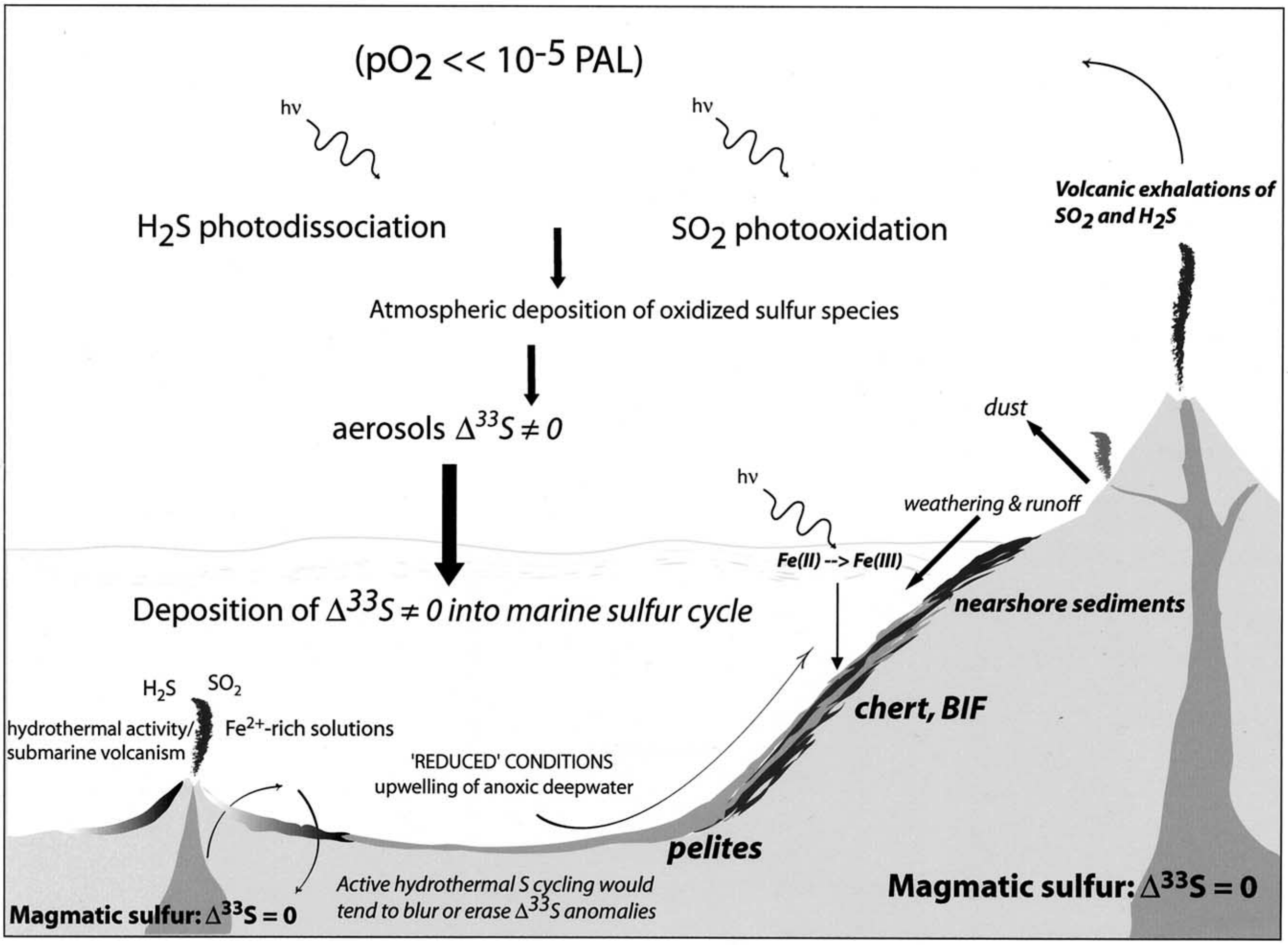

Fig. 17. A schematic model of early Archean sulfur cycles based on the results of this study and incorporating the work of Farquhar et al. (2000, 2001a) and Pavlov and Kasting (2002).

minimum ages determined from precise U-Th-Pb zircon geochronology of intrusive granitoids that cross-cut (and thus postdate) the supracrustal rocks including quartzite/BIF. On Akilia, two separate intrusive sheets of tonalitic orthogneiss appear to cross-cut the supracrustal package and include igneous zircons that can be dated. The ages of igneous cores in zircons from high-grade metamorphic rocks (including granulites and charnockites; Mojzsis et al., 2003) can be distinguished from younger overgrowths formed during later metamorphic events by in situ ion microprobe analyses (Compston et al., 1986; Compston and Kröner, 1988) especially when coupled with zircon U-Th-Pb depth-profiling and whole-rock geochemistry (Mojzsis and Harrison, 2002a). Such dating of the Akilia intrusive orthogneisses has yielded consistent 3830 ± 10 Ma ages, which are interpreted to be the crystallization age of the high-temperature protoliths of the gneissic sheets (Nutman et al., 1997a; Mojzsis and Harrison, 2002a). Hence, 3820 Ma is arguably a minimum limit on the depositional age of the sediments on Akilia, the oldest recognized thus far. These sediments have been used to infer a minimum age for the appearance of life on Earth, from measurements on carbon isotopic fractionations in graphite (Mojzsis et al., 1996), as well as to investigate the earliest environments for life in the context of conditions unique to the earliest Earth (Mojzsis and Harrison, 2000) such as the late heavy bombardment (Anbar et al., 2001; Mojzsis and Ryder, 2001).

4.3.2. *Metamorphic overprinting*

The metamorphic transition from amphibolite (in the Isua district of West Greenland) to the granulite facies that dominates the early Archean in coastal southern West Greenland (Griffin et al., 1980) is marked by dehydration and subsequent growth of orthopyroxene at the expense of amphibole (and biotite, where present). A number of studies have debated the degree to which the granulite transition, essential for stabilizing the deep continental crust, results from magmatic exhalations or from massive infiltration by CO_2 (Newton, 1986; Valley et al., 1990) or hypersaline fluids (Newton et al., 1998) derived from metamorphic devolatilization reactions. The presence of isolated ~500 to 900 μm sulfide grains in the Akilia quartzite described in this work, which compose ~0.1 mode % of the mineral assemblage, indicates that metamorphic fluids in the rock contained only small amounts of H_2S or SO_2 (Ohmoto, 1986). Because fluids with a juvenile S source derived from surrounding rocks should have $\Delta^{33}S = 0‰$, massive metasomatic infiltration by S-bearing fluids would be expected to blur or erase MIF anomalies if they were originally present. The anomalous $\Delta^{33}S$ data reported for *GR9707* are consistent with the deposition of MIF sulfur aerosols in a marine system and subsequent incorporation into the Akilia sediments. The fact that mass-independent sulfur isotope anomalies are preserved even into the granulite facies attests to the robustness of the $\Delta^{33}S$ signal in the absence of massive sulfidic overprinting that would otherwise dilute and ultimately erase MIF sulfur signatures.

4.3.3. Protolith to the Akilia Quartzite

Recently, the interpretation of a primary sedimentary origin of the Akilia quartzite has been disputed on the basis that the rocks could have been derived from metasomatic alteration of primary ultramafic + carbonate rocks (Fedo and Whitehouse, 2002a,b). However, this viewpoint has been challenged on geochemical (Mojzsis and Harrison, 2002b), mineralogical (Palin, 2002) and structural grounds (Friend et al., 2002). Because of the importance of these rocks to understanding Earth history as well as the criticisms raised over interpretations of their petrogenesis, it makes sense to explore the matter with a new approach. Therefore, on the basis of models for the origin of BIF discussed previously, we tested the hypothesis that the sulfides in this rock sampled either atmospheric (i.e., anomalous $\Delta^{33}S$) or magmatic exhalative sources ($\Delta^{33}S = 0‰$) of sulfur to the oceans at time of deposition in the early Archean $>$3.83 Ga. The $\Delta^{33}S$ data presented here (Table 4; Fig. 14) from a quartz-magnetite (*GR9707*) lithology on Akilia transcend different interpretations of the data of Fedo and Whitehouse (2002a) and provide support for a primary sedimentary origin of the Akilia quartzite.

5. CONCLUSIONS

We have presented new ion microprobe multicollector data measured for $\Delta^{33}S$ in sulfides derived from Archean sedimentary rocks. These results provide an independent verification of previous measurements of $\Delta^{33}S$ anomalies (Farquhar et al., 2000, 2001a,b; Thiemens et al., 2001) that hold the potential to constrain the chemistry of ancient atmospheres. The $\Delta^{33}S$ anomalies in terrestrial and extraterrestrial samples (Greenwood et al., 2000) are identifiable at the scale of the ion microprobe beam ($<30\ \mu m$) in individual sulfide grains and are resolvable from $\delta^{34}S/\delta^{33}S$ ratios on the (terrestrial) mass-fractionation line at a level of $\sim$0.2‰. The fractionations in $\delta^{34}S/\delta^{33}S$ observed in Archean sedimentary precipitates such as cherts (*PB6*), BIFs (*BH1*, *GR97im23*) and quartzite (*GR9707*), as well as a ferruginous metapelite (*GR97im43*) provide compelling evidence that most of the sulfur in these rocks passed through the atmosphere (Fig. 17). The simplest route taken by this anomalous sulfur would have been via SO_2 and/or H_2S from volcanic sources, followed by photochemical transformations in an anoxic atmosphere that imparted MIF to these gaseous species, and later deposition in the oceans probably as sulfur aerosols (Pavlov and Kasting, 2002) before conversion to sulfide. Our ion microprobe data are consistent with laboratory studies that propose that the operative photochemistry for MIF sulfur isotope reactions occurs under high-ultraviolet conditions deep in the atmosphere (Farquhar et al., 2001a) and $[pO_2]_{atm} \ll 10^{-5}$ PAL (Pavlov and Kasting, 2002). Thus, we conclude that our data are not consistent with oxygen levels above 10^{-5} PAL for the Archean atmosphere. A surprising conclusion from this work is that the majority of sulfur contained in the Archean sulfides we investigated must have had a significant residence time in the atmosphere, rather than being derived exclusively and directly from marine volcanic exhalations and hydrothermal fluids that would tend to blur or erase $\Delta^{33}S$ signatures. We have increased the data set for $\Delta^{33}S$ in pre-2.5 Ga sediments and have extended these measurements to the oldest sediments known; such $\Delta^{33}S$ anomalies are probably common or even abundant in early Precambrian sediments.

The ion microprobe multicollector technique provides an improved degree of spatial resolution that can be applied to specific sample sets, such as sediments spanning the 2.4- to 1.9-Ga "Great Oxidation Event" at the Archean–Proterozoic transition (Sleep, 2001). Many of the marine shales and carbonates from that time period contain abundant sulfides (Karhu, 1993; Karhu and Holland, 1996). We have shown how the spatial selectivity of multicollector SIMS facilitates measurement of $\Delta^{33}S$ at the scale of individual sulfide minerals and it is evident how this can be used in sediment cores, sulfidic microbands, and possibly microfossil forms where they are preserved and interpretable. Thus, the technique could be a useful tool for describing the rate function and timescale of oxygen increase in the early Proterozoic that we anticipate was inversely related to $\Delta^{33}S$ over time, as well exploring the mode of sulfur metabolisms of early life.

Acknowledgments—Technical assistance from G. Jarzebinski is gratefully appreciated. We thank D. Crowe and M. Chaussidon for donation of sulfide standards. Discussions with A. D. Anbar, Z. Crawford, J. Farquhar, H. D. Holland, M. Humayun, A. J. Kaufman, J. Karhu, D. Papineau, A. Pavlov, and B. Runnegar about this work have been helpful. We are grateful to Norm Pace for access to Archaea and Bacteria molecular phylogenies. Constructive reviews by J. Farquhar and two anonymous referees improved the article. This work was supported by the National Science Foundation grants EAR9978241, EAR9794651, and EAR0228999 (to S.J.M.) and by the NASA Astrobiology Institute. Field studies in West Greenland were also supported in part by the Isua Multidisciplinary Research Project directed by P. Appel, the Greenland Minerals Office and the Geological Survey of Denmark and Greenland. Facility support to the UCLA ion microprobe center comes from the Instrumentation and Facilities Program of the National Science Foundation.

Associate editor: F. Podosek

REFERENCES

Aggarwal P. K. and Nesbitt B. E. (1987) Pressure and temperature conditions of metamorphism in the vicinity of three massive sulfide deposits, Flin Flon–Snow Lake belt, Manitoba. *Can. J. Earth Sci.* **24,** 2305–2315.

Allaart J. H. (1976) The pre-3760 m.y. old supracrustal rocks of the Isua area, central West Greenland, and the associated occurrence of quartz-banded ironstone. In *The Early History of the Earth* (ed. B. F. Windley) pp. 177–189. Wiley.

Anbar A. D., Zahnle K. J., Arnold G. L., and Mojzsis S. J. (2001) Extraterrestrial iridium, sediment accumulation and the habitability of the early Earth's surface. *J. Geophys. Res.* **106,** 3219–3236.

Ault W. V. and Jensen M. L. (1962) Summary of sulfur isotope standards. In *Biogeochemistry of Sulfur Isotopes: National Science Foundation Symposium Proceedings*(ed. M. L. Jensen), pp. 16–29. Yale University Press.

Bao H., Thiemens M. H., Farquhar J., Campbell A. D., Lee C. W. C., Heine K., and Lope D. D. (2000) Anomalous ^{17}O compositions in massive sulphate mineral deposits on the Earth. *Nature* **406,** 176–178.

Barnicoat A. C., Henderson I. H. C., Knipe R. J., Yardley B. W. D., Napier R. W., Fox N. P. C., Kenyon A. K., Muntingh D. J., Strydom D., Winkler K. S., Lawrence S. R., and Cornford C. (1997) Hydrothermal gold mineralization in the Witwatersrand basin. *Nature* **386,** 820–824.

Beaudoin G., Taylor B. E., Rumble D., and Thiemens M. (1994) Variations in the sulfur isotope composition of troilite from the Canon Diablo iron meteorite. *Geochim. Cosmochim. Acta* **58,** 4253–4255.

Berner R. A. and Petsch S. T. (1998) The sulfur cycle and atmospheric oxygen. *Science* **282,** 1426–1427.

Bigeleisen J. and Mayer M. G. (1947) Calculation of equilibrium constants for isotopic exchange reactions. *J. Chem. Phys.* **15,** 261–267.

Bjerrum C. J. and Canfield D. E. (2002) Ocean productivity before about 1.9 Gyr ago limited by phosphorus adsorption onto iron oxides. *Nature* **417,** 159–162.

Braterman P. S., Cairns-Smith A. G., and Sloper R. W. (1983) Photooxidation of hydrated Fe^{2+}—Significance for banded iron formations. *Nature* **303,** 163–164.

Bridgwater D. and McGregor V. R. (1974) Fieldwork in the very early Precambrian rocks of the Isua area, southern West Greenland. *Rapp. Grønlands Geol. Unders.* **65,** 49–53.

Canfield D. E. and Raiswell R. (1999) The evolution of the sulfur cycle. *Am. J. Sci.* **299,** 697–723.

Chaussidon M. (1988) Géochimie du soufre dans le manteau et la croûte océanique: Apports de l'analyse isotopique in situ par sonde ionique. Ph.D. dissertation. Centre de Recherches Pétrographiques et Géochimiques, CNRS.

Cloud P. E. (1972) A working model of the primitive Earth. *Am. J. Sci.* **272,** 537–548.

Compston W., Kinny P. D., Williams I. S., and Foster J. J. (1986) The age and lead-loss behaviour of zircons from the Isua supracrustal belt as determined by ion microprobe. *Earth Planet. Sci. Lett.* **80,** 71–81.

Compston W. and Kröner A. (1988) Multiple zircon growth within early Archaean tonalitic gneiss from the Ancient gneiss complex, Swaziland. *Earth Planet. Sci. Lett.* **87,** 13–28.

Crowe D. E. and Vaughan R. G. (1996) Characterization and use of isotopically homogenous standards for in situ laser microprobe analysis of ^{34}S/^{32}S ratios. *Am. Mineral.* **81,** 187–193.

DesMarais D. J. (1997) Long-term evolution of the biogeochemical carbon cycle. *Rev. Mineral.* **35,** 429–448.

Dimroth E. and Kimberley M. M. (1976) Precambrian atmospheric oxygen: Evidence in the sedimentary distribution of carbon, sulfur, uranium and iron. *Can. J. Earth Sci.* **13,** 1161–1185.

Ding T., Valkiers S., Kipphardt H., De Bièvre P., Taylor P. D. P., Gonfiantini R., and Krouse R. (2001) Calibrated sulfur isotope abundance ratios of three IAEA sulfur isotope reference materials and V-CDT with a reassessment of the atomic weight of sulfur. *Geochim. Cosmochim. Acta* **65,** 2433–2437.

Dymek R. F. and Klein C. (1988) Chemistry petrology, and origin of banded iron-formation lithologies from the 3800 Ma Isua supracrustal belt, West Greenland. *Precambrian Res.* **39,** 247–302.

Farquhar J., Bao H., and Thiemens M. (2000) Atmospheric influence of Earth's earliest sulfur cycle. *Science* **289,** 756–758.

Farquhar J., Savarino J., Airieau S., and Thiemens M. H. (2001a) Observation of wavelength-sensitive mass-independent sulfur isotope effects during SO_2 photolysis: Implications for the early atmosphere. *J. Geophys. Res.* **106,** 32829–32839.

Farquhar J., Bao H. M., Thiemens M. H., Hu G. X., and Rumble D. (2001b) Questions regarding Precambrian sulfur isotope fractionation—Response. *Science* **292,** 1959.

Fedo C. M., Myers J. S., and Appel P. W. U. (2001) Depositional setting and paleographic implications of Earth's oldest supracrustal rocks, the $>$ 3.7 Ga Isua Greenstone belt, West Greenland. *Sed. Geol.* **141,** 61–77.

Fedo C. M. and Whitehouse M. J. (2002a) Metasomatic origin of quartz-pyroxene rock, Akilia, Greenland, and implications for Earth's earliest life. *Science* **296,** 1448–1452.

Fedo C. M. and Whitehouse M. J. (2002b) Origin and significance of Archean quartzose rocks at Akilia, Greenland—Response. *Science* **298,** 917a.

Forrest J. and Newman L. (1977) Silver-110 microgram sulfate analysis for the short time resolution of ambient level of sulfur aerosol. *Anal. Chem.* **49,** 1579–1584.

Friend C. R. L., Nutman A. P., and Bennett V. C. (2002) Origin and significance of Archean quartzose rocks at Akilia, West Greenland. *Science* **298,** 917a.

Gao X. and Thiemens M. H. (1993) Isotopic composition and concentration of sulfur in carbonaceous chondrites. *Geochim. Cosmochim. Acta* **57,** 3159–3169.

Goodwin A. M., Monster J., and Thode H. G. (1976) Carbon and sulfur isotope abundances in Archean iron-formations and early Precambrian life. *Econ. Geol.* **71,** 870–891.

Greenwood J. P., Mojzsis S. J., and Coath C. D. (2000) Sulfur isotopic compositions of individual sulfides in martian meteorites ALH84001 and Nakhla: Implications for crust-regolith exchange on Mars. *Earth Planet. Sci. Lett.* **184,** 23–35.

Griffin W. L., McGregor V. R., Nutman A. P., Taylor P. N., and Bridgwater D. (1980) Early Archaean granulite-facies metamorphism south of Ameralik, West Greenland. *Earth Planet. Sci. Lett.* **50,** 59–74.

Grinenko V. A. and Thode H. G. (1970) Sulfur isotope effects in volcanic gas mixtures. *Can. J. Earth Sci.* **7,** 1402–1409.

Holland H. D. (1984) *The Chemical Evolution of the Atmosphere and Oceans.* Princeton University Press.

Holland H. D. (1994) Early Proterozoic atmospheric change. In *Early Life on Earth: Nobel Symposium No. 84* (ed. S. Bengtson), pp. 237–244. Columbia.

Holland H. D. (1999) When did the Earth's atmosphere become oxic? A reply. *Geochem. News* **100,** 20–22.

Hulston J. R. and Thode H. G. (1965) Variations in the S^{33}, S^{34}, and S^{36} contents of meteorites and their relation to chemical and nuclear effects. *J. Geophys. Res.* **70,** 3475–3484.

Ireland T. R. (1995) Ion microprobe mass spectrometry: Techniques and applications in Cosmochemistry, geochemistry and geochronology. *Adv. Anal. Chem.* **2,** 1–118.

Karhu J. A. (1993) Paleoproterozoic evolution of the carbon isotope ratios of sedimentary carbonated in the Fennoscandian Shield. *Geol. Surv. Finland Bull.* **371,** 87.p.

Karhu J. A. and Holland H. D. (1996) Carbon isotopes and the rise of atmospheric oxygen. *Geology* **24,** 867–870.

Kasting J. F. (1992) Models related to Proterozoic atmospheric and ocean chemistry. In *The Proterozoic Biosphere: A Multidisciplinary Study* (eds. J. W. Schopf and C. Klein), pp. 1185–1187. Cambridge.

Kasting J. F. (1993) Earth's early atmosphere. *Science* **259,** 920–926.

Kasting J. F. (2001) The rise of atmospheric oxygen. *Science* **293,** 819–820.

Komiya T., Maruyama S., Masuda T., Nohda S., Hayashi M., and Okamoto K. (1999) Plate tectonics at 3.8–3.7 Ga: Field evidence from the Isua accretionary complex, southern West Greenland. *J. Geol.* **107,** 515–554.

Maruyama S., Masuda S., and Appel P. W. U. (1991) The oldest accretionary complex on the Earth, Isua, Greenland (abstract). *Geol. Soc. Am. Abs. Prog.* **23,** A429–A430.

McEwing C. E., Rees C. E., and Thode H. G. (1983) Sulphur isotope ratios in the Canyon Diablo metallic spheroids. *Meteoritics* **18,** 171–178.

McGregor V. R. and Mason B. (1977) Petrogenesis and geochemistry of metabasaltic and metasedimentary enclaves in the Amîtsoq gneisses, West Greenland. *Am. Mineral.* **62,** 887–904.

Millero F. and Sohn M. L. (1992) *Chemical Oceanography.* CRC Press.

Mojzsis S. J., Arrhenius G., McKeegan K. D., Harrison T. M., Nutman A. P., and Friend C. R. L. (1996) Evidence for life on Earth before 3,800 million years ago. *Nature* **384,** 55–59.

Mojzsis S. J. and Harrison T. M. (2000) Vestiges of a beginning: Clues to the emergent biosphere recorded in the oldest known sedimentary rocks. *Geol. Soc. Am. Today* **10,** 1–6.

Mojzsis S. J. and Ryder G. (2001) Accretion to Earth and Moon ~3.85 Ga. In *Accretion of Extraterrestrial Matter throughout Earth's His-*

tory (eds. B. Peucker-Ehrenbrink and B. Schmitz), pp. 423–446. Kluwer.

Mojzsis S. J. and Harrison T. M. (2002a) Establishment of a 3.83 Ga magmatic age for the Akilia tonalite (southern West Greenland). *Earth Planet. Sci. Lett.* **202,** 563–576.

Mojzsis S. J. and Harrison T. M. (2002b) Origin and Significance of. Archean quartzose rocks at Akilia, Greenland. *Science* **298,** 917a.

Mojzsis S. J., Devaraju T. C., and Newton R. C. (2003) Ion microprobe U-Pb age determinations on zircon from the Late Archean granulite facies transition zone of southern Karnataka, India. *J. Geol.,* in press.

Monster J., Appel P. W. U., Thode H. G., Schidlowski M., Carmichael C. M., and Bridgwater D. (1979) Sulfur isotope studies in early Archaean sediments from Isua, West Greenland—Implications for the antiquity of bacterial sulfate reduction. *Geochim. Cosmochim. Acta* **43,** 405–413.

Myers J. S. (2001) Protoliths of the 3.8–3.7 Ga Isua greenstone belt, West Greenland. *Precambrian Res.* **105,** 129–141.

Newton R. C. (1986) Fluids in granulite facies metamorphism. In *Fluid–Rock Interactions during Metamorphism* (eds. J. V. Walther and B. J. Wood), pp. 36–59. Springer-Verlag.

Newton R. C., Aranovichm L. Y., Hansen E. C., and Vandenheuvel B. A. (1998) Hypersaline fluids in Precambrian deep-crustal metamorphism. *Precambrian Res.* **91,** 41–63.

Nielsen H. (1979) Sulfur isotopes. In *Lectures in Isotope Geology* (eds. E. Jäger and J. C. Hunziger), pp. 283–312. Springer.

Nutman A. P., Allaart J. H., Bridgwater D., Dimroth E., and Rosing M. (1984) Stratigraphic and geochemical evidence for the depositional environment of the Early Archaean Isua supracrustal belt, southern West Greenland. *Precambrian Res.* **25,** 365–396.

Nutman A. P., McGregor V. R., Friend C. R. L., Bennett V. C., and Kinny P. D. (1996) The Itsaq Gneiss Complex of southern West Greenland: The world's most extensive record of early crustal evolution (3,900–3,600 Ma). *Precambrian Res.* **78,** 1–39.

Nutman A. P., Mojzsis S. J., and Friend C. R. L. (1997a) Recognition of ≥3850 Ma water-lain sediments in West Greenland and their significance for the early Archaean Earth. *Geochim. Cosmochim. Acta* **61,** 2475–2484.

Nutman A. P., Bennett V. C., Friend C. R. L., and Rosing M. T. (1997b) ~3710 and ≥3790 Ma volcanic sequences in the Isua (Greenland) supracrustal belt: structural and Nd isotope implications. *Chem. Geol.* **141,** 271–287.

Ohmoto H. (1986) Stable isotope geochemistry of ore deposits. In *Stable Isotopes in High Temperature Geological Processes* (eds. J. W. Valley, H. P. Taylor, and J. R. O'Neil), pp. 491–559. Reviews in Minerology 16. Mineralogical Society of America.

Ohmoto H. (1996) Evidence in pre-2.2 Ga paleosols for the early evolution of atmospheric oxygen and terrestrial biota. *Geology* **24,** 1135–1138.

Ohmoto H. (1999) When did the Earth's atmosphere become oxic? *Geochem. News* **93,** 12–27.

Ohmoto H. and Rye R. O. (1979) Isotopes of sulfur and carbon. In *Geochemistry of Hydrothermal Ore Deposits,* 2nd ed. (ed. H. L. Barnes), pp. 509–567. Wiley.

Ohmoto H., Yamaguchi K., and Ono S. (2001) Questions regarding Precambrian sulfur isotope fractionation. *Science* **292,** 1959a.

Oversby V. M. (1976) Isotopic ages and geochemistry of Archean acid igneous rocks from the Pilbara, Western Australia. *Geochim. Cosmochim. Acta* **40,** 817–829.

Pace N. R. (1997) A molecular view of microbial diversity and the biosphere. *Science* **276,** 734–740.

Pace N. R. (2001) The universal nature of biochemistry. *Proc. Natl. Acad. Sci. USA* **98,** 805–808.

Palin J. M. (2002) The origin of a most contentious rock. *Science* **298,** 961.

Pavlov A. A. and Kasting J. F. (2002) Mass-independent fractionation of sulfur isotopes in Archean sediments: Strong evidence for an anoxic Archean atmosphere. *Astrobiology* **2,** 27–41.

Pidgeon R. T. (1978) 3450-My-old volcanics in Archaean layered greenstone succession of Pilbara Block, Western Australia. *Earth Planet. Sci. Lett.* **37,** 421–428.

Rasmussen B. (2000) Filamentous microfossils in a 3,235-million-year-old volcanogenic massive sulphide deposit. *Nature* **405,** 676–679.

Rasmussen B. and Buick R. (1999) Redox state of the Archean atmosphere: Evidence from detrital heavy minerals in ca. 3250–2750 Ma sandstones from the Pilbara Craton, Australia. *Geology* **27,** 115–118.

Riciputi L. R. (1996) A comparison of extreme energy filtering and high mass resolution techniques for the measurement of $^{34}S/^{32}S$ ratios by ion microprobe. *Rapid Comm. Mass. Spec.* **10,** 282–286.

Riciputi L. R., Paterson B. A., and Ripperdan R. L. (1998) Measurements of light stable isotope ratios by SIMS: Matrix effects for oxygen, carbon, and sulfur isotopes in minerals. *Int. J. Mass Spec.* **178,** 81–112.

Rose N. M., Rosing M. T., and Bridgwater D. (1996) The origin of metacarbonate rocks in the Archaean Isua supracrustal belt, West Greenland. *Am. J. Sci.* **296,** 1004–1044.

Rosing M. T., Rose N. M., Bridgwater D., and Thomsen H. S. (1996) Earliest part of Earth's stratigraphic record: A reappraisal of the >3.7 Ga Isua (Greenland) supracrustal sequence. *Geology* **24,** 43–46.

Rumble D., Hoering T. C., and Palin J. M. (1993) Preparation of SF_6 for sulfur isotope analysis by laser-heating sulfide minerals in the presence of F_2 gas. *Geochim. Cosmochim. Acta* **57,** 4499–4512.

Rye R. O. and Holland H. D. (1998) Paleosols and the evolution of atmospheric oxygen: A critical review. *Am. J. Sci.* **298,** 621–672.

Rye R., Kuo P. H., and Holland H. D. (1997) Atmospheric carbon dioxide concentrations before 2.2 billion years ago. *Nature* **378,** 603–605.

Schidlowski M., Hayes J. M., and Kaplan I. R. (1983) Isotopic inferences of ancient biochemistries. Carbon, sulfur, hydrogen and nitrogen. In *Earth's Earliest Biosphere—Its Origin and Evolution* (ed. J. W. Schopf), pp. 149–186. Princeton University Press.

Schidlowski M. (1989) Evolution of the sulphur cycle in the Precambrian. In *Evolution of the Global Biogeochemical Sulphur Cycle* (ed. P. Brimblecomb and A. Yu. Lein), pp. 3–19. Wiley.

Shen Y., Buick R., and Canfield D. E. (2001) Isotopic evidence for microbial sulphate reduction in the early Archaean era. *Nature* **410,** 77–81.

Sleep N. (2001) Oxygenating the atmosphere. *Nature* **410,** 317–319.

Stetter K. O. (1996) Hyperthermophiles in the history of life. In *Evolution of Hydrothermal Systems on Earth (and Mars?)* (eds. G. R. Bock and J. A. Goode), pp. 1–10. Wiley.

Stetter K. O. and Gaag G. (1983) Reduction of molecular sulphur by methanogenic bacteria. *Nature* **305,** 309–311.

Strauss H. and Moore T. B. (1992) Abundances and isotopic compositions of carbon and sulfur species in whole rock and kerogen. In *The Proterozoic Biosphere.* (eds. J. W. Schopf and C. Klein), pp. 709–798. Cambridge University Press.

Sugitani K. (1992) Geochemical characteristics of Archean cherts and other sedimentary rocks in the Pilbara Block, Western Australia: Evidence for Archean seawater enriched in hydrothermally-derived iron and silica. *Precambrian Res.* **57,** 21–47.

Thiemens M. H. (1999) Mass-independent isotope effects in planetary atmospheres and the early solar system. *Science* **283,** 341–345.

Thiemens M. H., Savarino J., Farquhar J., and Bao H. (2001) Mass-independent isotopic compositions in terrestrial and extraterrestrial solids and their implications. *Acc. Chem. Res.* **34,** 645–652.

Thode H. G., Macnamara J., and Collins C. B. (1949) Natural variations in the isotopic content of sulphur and their significance. *Can. J. Res.* **27B,** 361.

Thrope R. I., Hickman A. H., Davis D. W., Mortensen J. K., and Trendall A. F. (1992) U-Pb zircon geochronology of Archean felsic units in the Marble Bar region, Pilbara Craton, Western Australia. *Precambrian Res.* **56,** 169–189.

Towe K. M. (1990) Aerobic respiration in the Archaean. *Nature* **348,** 54–56.

Trendall A. F. and Morris R. C. (1983) *Iron Formations: Facts and Problems.* Elsevier.

Valley J. W., Bohlen S. R., Essene E. J., and Lamb W. (1990) Metamorphism in the Adirondacks II. The role of fluids. *J. Petrol.* **31,** 555–596.

Walker J. C. G. (1977) *Evolution of the Atmosphere.* Macmillan.

Walker J. C. G., Klein C., Schidlowski M., Schopf J. W., Stevenson D. J., and Walter M. R. (1983) Environmental evolution of the Archean–Early Proterozoic Earth. In *Earth's Earliest Biosphere: Its Origin and Evolution* (ed. J. W. Schopf), pp. 260–290. Princeton.

Watanabe K., Naraoka H., Wronkiewicz D. J., Condie K. C., and Ohmoto H. (1997) Carbon, nitrogen, and sulfur geochemistry of the

Archean and Proterozoic shales from the Kaapvaal Craton, South Africa. *Geochim. Cosmochim. Acta* **61,** 3441–3459.

Whelan J. F., Rye R. O., and deLorraine W. (1984) The Balmat-Edwards zinc-lead deposits: Synsedimentary ore from Mississippi Valley-type fluids. *Econ. Geol.* **79,** 239–265.

Woese C. R. (1987) Bacterial evolution. *Microbiol. Rev.* **51,** 221–271.

Woese C. R. (2000) Interpreting the universal phylogenetic tree. *Proc. Natl. Acad. Sci. USA* **97,** 8392–8396.

Young E. D., Galy A., and Nagahara H. (2002) Kinetic and equilibrium mass-dependent isotope fractionation laws in nature and their geochemical and cosmochemical significance. *Geochim. Cosmochim. Acta* **66,** 1095–1104.

Zinner E. (1989) Isotopic measurements with the ion microprobe. In *New Frontiers in Stable Isotope Research: Laser Probes, Ion Probes and Small-Sample Analysis* (eds. W. C. Shanks III and R. E. Criss), pp. 145–162. Bulletin 1890. U.S. Geological Survey.